NUWC-NPT Technical Report 11,467
15 August 2005

A Thermal Analysis of High-Drive Ring Transducer Elements

Stephen C. Butler
John B. Blottman III
Robert E. Montgomery
Sensors and Sonar Systems Department

NEWPORT

Naval Undersea Warfare Center Division
Newport, Rhode Island

PREFACE

The research described in this report was performed under NUWC Division Newport Project No. TD0951, "Affordable Common Devices," principal investigator Stephen C. Butler (Code 1516), program manager Richard Schmidt (Code 824), systems engineering manager Gerald T. Stevens (Code 8211), and transducer and amplifier and task manager Frank A. Tito (Code 1516). This research was initially sponsored by the Office of Naval Research (ONR-333); it was completed under the ONR-sponsored "High-Powered Source" program (ONR-321).

The technical reviewer for this report was Kim D. Gittings (Code 1516).

The authors thank Jan F. Lindberg (ONR-321MS) and Patrick J. Monahan and Michael D. Jevnager (both NUWC Code 1516) for their support and assistance.

Reviewed and Approved: 15 August 2005

Joseph M. Monti

Joseph M. Monti
Head, Sensors and Sonar Systems Department

TABLE OF CONTENTS

TABLE OF CONTENTS (Cont'd)

Section **Page**

LIST OF ILLUSTRATIONS

Figure **Page**

LIST OF ILLUSTRATIONS (Cont'd)

LIST OF ILLUSTRATIONS (Cont'd)

Figure **Page**

LIST OF TABLES

Table **Page**

LIST OF ABBREVIATIONS, ACRONYMS, AND SYMBOLS

A	Area (m^3)
A_c	Ceramic cylinder area (m^2)
A_p	Polymer area (m^2)
ac	Alternating current
APTF	Acoustic Pressure Tank Facility

LIST OF ABBREVIATIONS, ACRONYMS, AND SYMBOLS (Cont'd)

B	Susceptance (S)
B_i	Boit number
C	Specific heat (J/kg °C)
C_b	Clamped or blocked capacitance (farad)
C_f	Free capacitance (farad)
C_m	Mechanical compliance (m/N)
d	Thickness of polymer coating (m)
E	Electric field (rms) (V/m)
F	Force (N)
FE	Finite element
FEA	Finite element analysis
G	Conductance (S)
G_b	Electrical losses conductance (S)
h	Convection film coefficient (W/m^2 °C)
ID	Inner diameter
k	Thermal conductivity (W/m°C)
k_c	Thermal conductivity of piezoelectric ceramic (W/m °C)
K^T	Free dielectric constant
M	Mechanical mass (kg)
N	Electromechanical turns ratio
NUWC	Naval Undersea Warfare Center
OD	Outer diameter
P_a	Radiated acoustic output power (W)
P_e	Electrical power losses (W)
P_{in}	Dissipated electrical input power (W)
P_{loss}	Total dissipated power, electrical plus mechanical (W)
P_m	Mechanical power losses (W)
PZT	Lead zirconate titanate
q	Heat flux (W)
Q	Rate of internal heat generation (W/m^3)
Q_m	Mechanical quality factor
Q_w	In-water loaded mechanical quality factor
R_b	Electrical dissipative loss (ohm)
R_j	Damping loss $\left(N\frac{\text{sec}}{\text{m}}\right)$
R_L	Radiation resistance $\left(N\frac{\text{sec}}{\text{m}}\right)$
rms	Root mean square
S	Siemens
SS	Steady state
T	Temperature (°C)
t	Time (seconds)

LIST OF ABBREVIATIONS, ACRONYMS, AND SYMBOLS (Cont'd)

T_∞	Farfield fluid temperature (°C)
T_o	Initial temperature (°C)
τ_p	Inverse characteristic thermal conduction relaxation time constant for polymer
T^{ss}	Steady-state temperature (°C)
TVR	Transmit voltage response
u	Velocity (m/sec)
U	Internal energy (W/m^3)
V	Voltage
V_c	Ceramic cylinder volume (m^3)
V_c	Piezoelectric ceramic cylinder volume (m^3)
V_p	Polymer volume (m^3)
W	Watt
$2a$	Ceramic cylinder wall thickness (m)
$2L$	Ceramic cylinder height (m)
α	Thermal diffusivity (m^2/s)
$\tan \delta_e$	Dielectric loss factor
$\tan \delta_m$	Mechanical loss factor
ε_o	Dielectric constant of free space 8.854×10^{-12}
ω	Angular frequency (rad) $2\pi f$
ρ	Density (kg/m^3)
τ	Steady-state time constant (seconds)
τ_c	Inverse characteristic thermal conduction relaxation time constant for PZT
τ_h	Inverse characteristic thermal convection relaxation time constant for fluid

A THERMAL ANALYSIS OF HIGH-DRIVE RING TRANSDUCER ELEMENTS*

1. INTRODUCTION

Heat transfer characteristics are an important consideration for designers of new underwater, high-power sonar transducers. Of particular concern is the possible overheating of the active elements, such as the piezoelectric ceramics and the electrostrictive and magnetostrictive materials—all of which, when driven at full power, generate considerable heat. If the transducer configuration does not allow for adequate cooling, the active element may not perform properly or reliably, and its lifetime may be considerably shortened; in the worst-case scenario, the active element may be destroyed. Generally, for piezoelectric ceramics, the temperature should not exceed the Curie point (~300 °C); in fact, for reliable performance, the temperature should be held to levels 50% below the Curie point (reference 2).

Thermal issues are most often prevalent when the active elements are encased in an insulating blanket, usually polymer or a polymer-based composite material. The fact that these materials are good electrical insulators suggests that they are also good heat insulators.

The thermal performance of a particular transducer design is usually estimated by performing bench-top testing on individual components or by testing complete units under realistic conditions. Bench-top testing may yield data that do not correlate with the thermal behavior of a complete unit. Full-scale tests, on the other hand, should provide reliable data; however, this approach may be very expensive, especially if redesigns are required.

This report considers only piezoelectric ring transducers driven at high power levels under continuous sine-wave drive, which can create destructive temperatures in the active elements. The transducers consist of several piezoelectric ceramic cylinders of three sizes that are coated with a polymeric insulator as a water barrier (see references 3, 4, and 5) for designated operations. In-air testing of uncoated and coated ceramic cylinders was first performed to determine the temperature-versus-time profile for different drive levels. The results were used to help in developing analytical models that can predict temperature profiles of the transducers in water and to help in providing guidelines concerning thermal issues. The models complement the measurements and may be used to optimize material choices and to predict behavior under operational conditions.

---

*Portions of this report were presented at the *137th Meeting of the Acoustical Society of America*, Berlin, Germany, 14 – 19 March 1999 (see reference 1).

This report focuses on thermal models for a compact, high-drive, 31-mode, free-flooded ring underwater sonar transducer. For this type of transducer, it was found that, thermal issues—rather than electric field limits or mechanical stress limits—were the limiting design concern. The models that were developed are therefore based on dielectric losses in the ceramic material. The results are compared to measurement data and finite element (FE) model solutions. These models must address the transient temperature behavior because the application requires knowledge of the temperature as a function of time. Figure 1 shows the basic configuration of a radially poled, 31-mode piezoelectric cylinder that is addressed in this report.

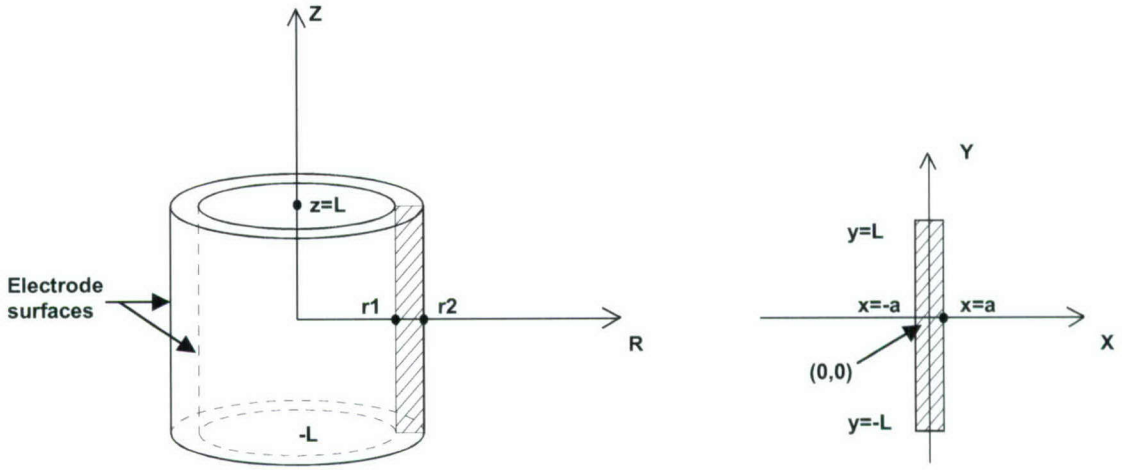

Figure 1. Radially Poled Piezoelectric Ceramic Cylinder

2. INPUT ELECTRICAL POWER

The radiated acoustic power P_a for a sonar transducer is the electrical input power P_{in} minus its dissipated inertial power losses P_{loss}; that is,

$$P_a = P_{in} - P_{loss}. \tag{1}$$

The electroacoustic efficiency is given by

$$\eta_{ea} = \frac{P_a}{P_{in}}. \tag{2}$$

The total dissipated power loss in the transducer is represented by the internal electrical losses P_e and internal mechanical losses P_m and is given by

$$P_{loss} = P_e + P_m. \tag{3}$$

Total electrical power input P_{in} is thus equal to the internal electrical losses P_e, internal mechanical losses P_m, and radiated acoustic power P_a; that is,

$$P_{in} = P_e + P_m + P_a. \tag{4}$$

The mechanical losses may be associated with viscous losses, damping losses, and the elastic constants of the piezoelectric material tan δ_m (reference 6). For a piezoelectric ceramic cylinder, the viscous and damping losses are negligible and the mechanical losses are associated with the elastic constants, which are typically 0.0012 for PZT-8 and 0.0032 for PZT-4 at high electric-field drive conditions (reference 6). The $\tan\delta_m$ reciprocal value is commonly listed in the technical piezoelectric ceramics catalogs (as shown in references 7 – 10) for piezoelectric properties such as Q_m (mechanical quality factor) and is typically 1000 for PZT-8 and 500 for PZT-4 for low-signal drive conditions and 833 and 313, respectively, for high-signal drive conditions.

A piezoelectric sonar transducer can be represented by an equivalent electrical circuit to describe its behavior (see figure 2). Such a circuit comprises three sections: electrical impedance, mechanical impedance, and acoustic impedance. The electrical impedance section is composed of electrical leads, electrical dissipative losses R_b, and clamped or blocked capacitance C_b of the piezoelectric ceramic material.

The mechanical impedance section is composed of the mechanical vibrating components such as mass M and mechanical compliance C_m of a radially poled, 31-mode ceramic cylinder. The mechanical losses are denoted as viscous losses, damping losses R_j, and the elastic constants of the piezoelectric material R_m (reference 6).

The acoustic impedance section is the load impedance R_L exerted by the medium on the radiating surface area of the transducer. (The radiation impedance is a complex quantity; for this discussion, however, only the real part is addressed.) The electromechanical transformer in the circuit is given by the turns ratio 1:N, which converts the applied ac rms drive voltage V at the electrical terminals to an ac force F at the input to the mechanical section of the circuit. The force drives the mechanical component and produces a velocity u to the acoustic load R_L, which radiates acoustic output power P_a into the medium.

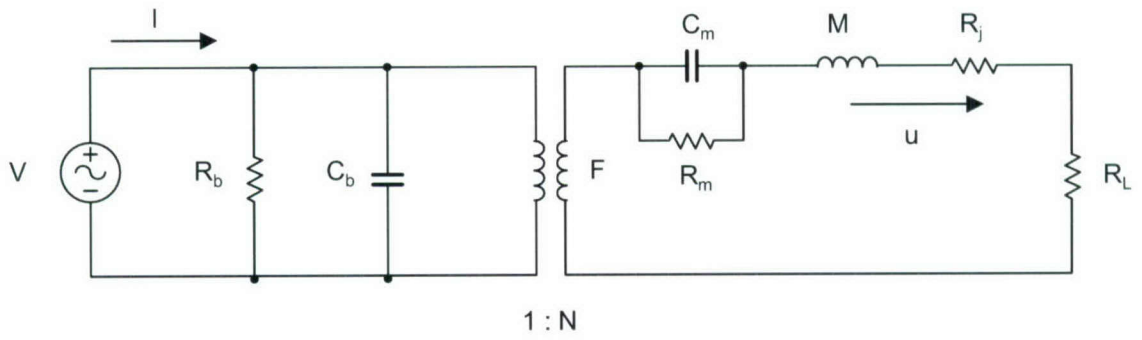

Figure 2. Generalized Equivalent Circuit Representation of a Piezoelectric Sonar Transducer

2.1 LOW-FREQUENCY APPROXIMATION

At low frequencies $1/\omega C_m >> \omega M$, where $\omega = 2\pi f$ is the angular frequency and $R_L \approx 0$ is the radiation acoustic load, the input electrical power becomes $P_{in} = P_{loss}$ since $P_a = 0$. The equivalent circuit reduces to that shown in figure 3.

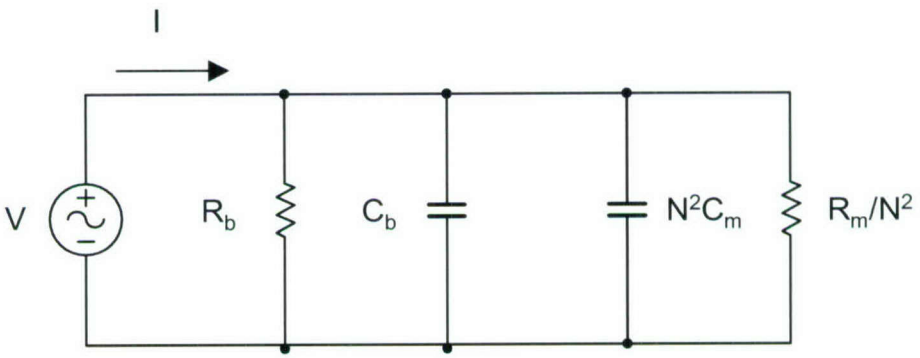

Figure 3. Equivalent Circuit Representation of a Piezoelectric Sonar Transducer at Low Frequency

The resulting complex circuit input admittance is defined as the ratio of drive current-to-drive voltage:

$$Y_{in} = \frac{I}{V} = G + jB = \left(G_b + \frac{N^2}{R_m} \right) + j\omega\left(C_b + N^2 C_m\right) = G_b + \frac{N^2}{R_m} + j\omega\left(C_f\right), \tag{5}$$

where

$G_b = 1/R_b$ and $C_f = C_b + N^2 C_m$.

The input power at low frequency, written as the real part of the admittance times the voltage squared, is

$$P_{in} = V^2 \left[G_b + \frac{N^2}{R_m} \right] = V^2 G_b + V^2 \frac{N^2}{R_m}. \tag{6}$$

The electrical dissipation factor $\tan \delta_e$ at low frequency is the ratio of electrical losses G_b across the total capacitance of the equivalent circuit:

$$\tan \delta_e = \frac{1}{\omega R_b (C_b + N^2 C_m)} = \frac{G_b}{\omega C_f}. \tag{7}$$

The mechanical dissipation factor $\tan \delta_m$ is associated with mechanical losses R_m and mechanical compliance C_m of the piezoelectric material:

$$\tan \delta_m = \frac{1}{\omega R_m C_m}; \tag{8}$$

therefore, P_{in} can now be expressed in terms of dissipation:

$$P_{in} = V^2 \omega \left[C_f \tan \delta_e + N^2 C_m \tan \delta_m \right]. \tag{9}$$

The effective coupling factor squared is defined as

$$k_{eff}^2 = \frac{N^2 C_m}{C_f}. \tag{10}$$

The power input is thus written as

$$P_{in} = V^2 \omega C_f \left[\tan \delta_e + k_{eff}^2 \tan \delta_m \right]. \tag{11}$$

Note that the rms electric field in the ceramic is $E = V/t$, and free capacitance is defined as $C_f = K^T \varepsilon_o A/t$, where K^T is the dielectric constant; therefore,

$$V^2 C_f = E^2 t^2 \frac{K^T \varepsilon_o A}{t} = E^2 K^T \varepsilon_o A t = E^2 K^T \varepsilon_o V_c, \tag{12}$$

and the input electrical power at low frequency is finally written as

$$P_{in} = \omega E^2 K^T \varepsilon_o V_c \tan \delta_e + \omega E^2 k_{eff}^2 K^T \varepsilon_o V_c \tan \delta_m. \tag{13}$$

In equation (13), V_c denotes the volume of piezoelectric ceramic.

In summary, at low frequency, consider the case where the transducer's coupling coefficient is low: the major portion of the dissipated power P_{loss} will be in the dielectric losses, as in a capacitor. Thus, for a ceramic cylinder with a coupling coefficient of 0.33, an electrical dielectric loss tangent factor of 0.0065, and a mechanical losses tangent factor of 0.0012—all typical for a 31-mode ceramic cylinder—98% of the input power is consumed by the dielectric losses and 2% of the input is consumed by the mechanical losses of the ceramic. If, however, the coupling coefficient is much higher (0.8, for example), 89% of the input power is consumed by the dielectric losses and 11% of the input is consumed by the mechanical losses of the ceramic—below resonance.

2.2 RESONANT DEVICE

In the generalized equivalent circuit (figure 2), the parallel combination of C_m and R_m can be combined into an impedance, as shown in equation (14):

$$Z_m = \frac{R_m \dfrac{1}{j\omega C_m}}{R_m + \dfrac{1}{j\omega C_m}} = \frac{\dfrac{1}{j\omega C_m}}{1 + \dfrac{1}{j\omega C_m R_m}} = \frac{\dfrac{1}{j\omega C_m}}{1 - j \tan \delta_m} = \frac{\dfrac{1}{j\omega C_m}(1 + j \tan \delta_m)}{1 + \tan^2 \delta_m}. \tag{14}$$

When $\tan\delta_m << 1$, the parallel impedance becomes a series impedance:

$$Z_m \approx \frac{1}{j\omega C_m} + \frac{\tan \delta_m}{\omega C_m} = \frac{1}{j\omega C_m} + R_c. \tag{15}$$

The mechanical dissipation factor can now be represented as

$$\tan \delta_m = \omega R_c C_m, \tag{16}$$

or by the circuit shown in figure 4.

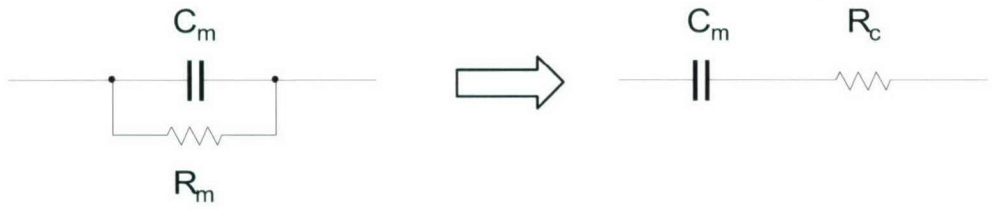

Figure 4. Parallel Impedance Transformed to a Series Impedance

At resonance, $1/\omega C_m = \omega M$ and the equivalent circuit in figure 2 reduces to that in figure 5.

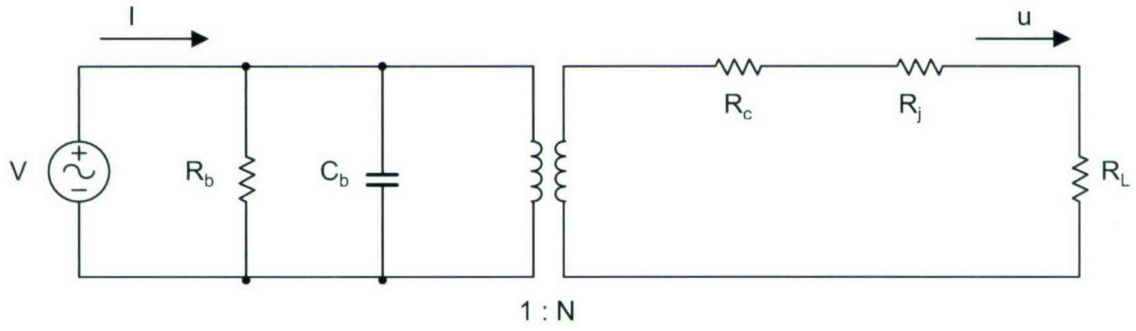

Figure 5. Equivalent Circuit at Resonance

The circuit input admittance at resonance now becomes

$$Y_{in}^{\omega_r} = G_b + \frac{N^2}{R_c + R_j + R_L} + j\omega C_b. \tag{17}$$

The input power at resonance, written as the real part of the admittance times the voltage squared, is, from equations (7) and (10)

$$P_{in} = V^2\left[G_b + \frac{N^2}{R_c + R_j + R_L}\right] = V^2\omega C_f \tan\delta_e + V^2 N^2 Q_w \omega C_m$$

$$= V^2\omega C_f \tan\delta_e + V^2 k_{eff}^2 C_f \omega Q_w$$

$$= V^2\omega C_f\left[\tan\delta_e + k_{eff}^2 Q_w\right], \tag{18}$$

where the in-water quality factor is defined as

$$Q_w = \frac{1}{\omega_r C_m (R_c + R_j + R_L)}. \tag{19}$$

The in-water loaded quality factor Q_w characterizes the sharpness of the transmitting pressure response of the transducer at its resonant frequency ω_r when the transducer is loaded in the water medium. C_m is the mechanical compliance of the ceramic cylinder. R_L is the in-water load resistance (density times the sound speed of the fluid medium times the acoustic radiating surface area of the ceramic cylinder), and R_c is the mechanical loss in the ceramic, as well as other mechanical losses R_j (viscous losses, damping losses, etc.).

Consider the case where $k_{eff}^2 Q_w >> 1$. The input electrical power is approximated as $P_{in} = V^2 \omega C_f k_{eff}^2 Q_w$ and is dominated by mechanical losses and acoustic radiation. Alternatively, if $k_{eff}^2 Q_w << 1$, the input power is approximated by $P_{in} = V^2 \omega C_f \tan \delta_e$, which is dominated by electrical losses.

Substituting the electric field and dielectric constant, equation (13) yields equation (20) for the input power at resonance:

$$P_{in} = \omega E^2 K^T \varepsilon_o V_c \tan \delta_e + \omega E^2 Q_w k_{eff}^2 K^T \varepsilon_o V_c. \tag{20}$$

The second term on the right side of equation (20) is the sum of dissipated mechanical and radiated acoustic power:

$$P_m + P_a = \omega E^2 Q_w k_{eff}^2 K^T \varepsilon_o V_c. \tag{21}$$

The first term on the right side of equation (20) is the electrical power losses of the piezoelectric ceramic material:

$$P_e = \omega E^2 V_c K^T \varepsilon_o \tan \delta_e. \tag{22}$$

The mechanical losses at resonance are a function of the strain in the piezoelectric material and are written as

$$P_m = \omega_r T^2 s^E V_c \tan \delta_m. \tag{23}$$

At low frequencies (that is, under free condition), the strain is $S = dE$; but at resonance the strain is amplified by Q_w. Hence, $S = dEQ_w$, and the stress becomes $T = S/s^E = EQ_w d/s^E$. The mechanical loss, therefore, may be written in terms of the quality factor and material constants:

$$P_m = \omega_r E^2 Q_w^2 d^2 s^E V_c \tan \delta_m, \tag{24}$$

where d is the piezoelectric strain coefficient and s^E is the short-circuit elastic modulus. Finally,

since $d^2 = k_{eff}^2 s^E K^T \varepsilon_o$, equation (24) becomes

$$P_m = \omega E^2 Q_w^2 k_{eff}^2 K^T \varepsilon_o V_c \tan \delta_m . \tag{25}$$

Table 1 lists the power contribution of the electrical and mechanical losses for loaded quality factors of 3 and 30, using equations (20), (22), and (25), for an ideal ceramic cylinder with a coupling coefficient of 0.33 and with other mechanical losses neglected, that is, $R_j = 0$. The dielectric and mechanical loss tangent factor values in table 1 are at the maximum electric field levels for a Navy Type III ceramic cylinder for these quality factors. The drive field levels are lower for the high quality factor because of stress limitation; if driven harder, the ceramic cylinder would go into tension and fracture. For a loaded quality factor of 3, the mechanical power losses are 10 times lower than the electrical power losses. The results reverse for a loaded quality factor of 30, where now the electrical losses are 10 times lower than the mechanical power losses (see also table 8 in reference 6).

Table 1. Power Contribution of the Electrical and Mechanical Losses for Low- and High-Load Quality Factors

Q_w	Field (kVrms/m)	$\tan\delta_e$	$\tan\delta_m$	P_{in} (W)	P_e (W)	P_m (W)	P_a (W)
3	400	0.01	0.0012	100	3.3	0.35	96.4
30	130	0.005	0.005	100	0.15	14.7	85.2

The data in table 1 demonstrate that internal dielectric losses are more important for lower loaded quality factors and the mechanical losses contribute more to higher load quality factors. Damping losses and other mechanical losses, such as viscous losses, would change the results and may equalize the contribution between electrical and mechanical losses for higher load quality factors. The in-water loaded quality factors for the ceramic cylinders used in this study are 3 (as reported in reference 5); thus, for the study reported in the following section, it was assumed that the mechanical losses are negligible and equation (22) was used as the source of dissipated heat in the analytical temperature models.

3. ANALYTICAL MODEL

The energy balance (heat flow) equation for a solid material is (reference 11)

$$\frac{\partial T}{\partial t} = \alpha \nabla^2 T + \frac{Q}{\rho C}, \tag{26}$$

where T = temperature (°C), t = time (sec), α = thermal diffusivity (m^2/s), ρ = density (kg/m^3), C = the specific heat (J/kg °C), and Q = the rate of internal heat generation (W/m^3). The diffusivity can be expressed as

$$\alpha = \frac{k}{\rho C}, \tag{27}$$

where k = the thermal conductivity (W/m °C).

Conduction in the solid requires that the heat flux in watts,

$$q = -kA\nabla T, \tag{28}$$

be continuous across any solid-solid interface of area A. At solid-fluid interfaces where convection is important, the heat flux can be expressed as

$$q = Ah(T - T_\infty), \tag{29}$$

where h = convection film coefficient (W/m^2 °C), T is the temperature at the interface, and T_∞ is the temperature in the fluid far removed from the interface. The rate of change of internal energy per unit volume (W/m^3) is given by

$$\frac{\partial U}{\partial t} = \rho C \frac{\partial T}{\partial t}. \tag{30}$$

The internal energy changes whenever there is a net influx/outflux of heat and/or when internal heat sources are present. In this study, the internal sources are the result of dielectric heating in the piezoelectric material, as given by equation (22). Dividing equation (22) by the ceramic volume gives the internal heat source in watts/volume:

$$Q = \omega E^2 \varepsilon^T \tan\delta_e, \tag{31}$$

where

$$\varepsilon^T = K^T \varepsilon_o. \tag{32}$$

The electric field may be written as $V/2a$, where V is the rms voltage across the electrodes, and $2a$ is the wall thickness of the ceramic cylinder.

Consider the ceramic cylinder shown in figure 1. The Laplacian in cylindrical coordinates is defined as

$$\nabla^2 T = \frac{\partial^2 T}{\partial r^2} + \frac{1}{r}\frac{\partial T}{\partial r} + \frac{1}{r^2}\frac{\partial^2 T}{\partial \theta^2} + \frac{\partial^2 T}{\partial z^2}. \tag{33}$$

For the case of axisymmetric geometry,

$$\frac{1}{r^2}\frac{\partial^2 T}{\partial \theta^2} = 0. \tag{34}$$

The Laplacian may be accurately modeled as a planar region if the Biot number is much less than 1 (reference 11). In this research, the Biot numbers for all cylinders studied are less than 0.05; thus, the Laplacian reduces to

$$\nabla^2 T = \frac{\partial^2 T}{\partial x^2} + \frac{\partial^2 T}{\partial y^2}, \tag{35}$$

where the Biot number Bi is a measure of the ratio of convection-to-conduction, defined as

$$Bi \equiv \frac{h(r_2 - r_1)}{k_c}, \tag{36}$$

where k_c is the thermal conductivity of the ceramic.

The heat flow equation (26) may be solved by the method of separation of variables. Let

$$T(x, y, t) = f(t)g(x, y). \tag{37}$$

Substituting equation (37) into equation (35) and taking a linear combination of solutions yields the complete analytical solution in the form

$$T(x,y,t) = \sum_{nm} A_{nm} \cos\left(\lambda_n \frac{x}{a}\right) \cos\left(\lambda_m \frac{y}{l}\right) \left[1 - e^{-k_{nm} t}\right], \tag{38}$$

where λ_n, λ_m, and k_{nm} are separation constants to be determined from the boundary conditions and the initial conditions. It is convenient to express the internal heat generation term in the same fashion by using equation (26); that is, let

$$\frac{Q}{\rho C} = \sum_{nm} B_{nm} \cos\left(\lambda_n \frac{x}{a}\right) \cos\left(\lambda_m \frac{y}{l}\right). \tag{39}$$

These expansions are valid provided that the individual terms are eigenfunctions of a linear Hermitian operator (reference 12). The boundary conditions that are used require that the expansions not be Fourier series; nevertheless, the eigenfunctions do form a complete orthonormal set in the interval $-a \le x \le a,\ -l \le y \le l$. Note that sine functions are excluded because of symmetry.

Substituting the analytical solution equation (38) and heat source equation (39) into the heat flow equation (26) yields

$$k^2_{nm} = \alpha \left(\frac{\lambda^2_n}{a^2} + \frac{\lambda^2_m}{l^2} \right), \tag{40}$$

and

$$A_{nm} = \frac{B_{nm}}{k^2_{nm}}. \tag{41}$$

To evaluate λ_n, λ_m, consider the boundary conditions. At $x = \pm a$, and at $y = \pm l$, heat is transferred to the fluid by conduction and convection according to equations (28) and (29), respectively. Thus, at the interface with the fluid, continuity of heat flux is required:

$$- k \frac{\partial T}{\partial x} = h \left[T - T_\infty \right], \tag{42}$$

$$- k \frac{\partial T}{\partial y} = h \left[T - T_\infty \right]. \tag{43}$$

Applying the analytical solution, equation (38), into equations (42 and 43) requires that

$$\cot \lambda_n = \left(\frac{k}{a\,h} \right) \lambda_n, \tag{44}$$

and

$$\cot \lambda_m = \left(\frac{k}{l\,h} \right) \lambda_m. \tag{45}$$

These equations must be evaluated numerically.

Assume that the rate of internal heat generation Q is uniform in the ceramic. Then, by using the principle of orthogonality of the eigenfunctions in equation (39), in a manner similar to evaluating the coefficients of a Fourier series, it is found that

$$B_{nm} = \frac{16\,Q \sin \lambda_n \sin \lambda_m}{\rho\, C\, [\, \sin 2\lambda_n + 2\, \lambda_n\,][\, \sin 2\lambda_m + 2\, \lambda_m\,]}. \tag{46}$$

By using equation (46), the A coefficients from equation (41) can now be determined. Equations (38) through (46) constitute a complete solution to the heat flow problem that satisfies the initial condition $T(t = 0) = 0$.

4. DISCUSSION OF THE SOLUTION

The solution to the heat flow equation (38) assumes that the initial temperature is zero. If this is not the case of interest, any value for the initial temperature T_o (temperature offset) may be added to the solution to obtain the correct result. For example,

$$T(x,y,t) = \sum_{nm} A_{nm} \cos(\lambda_n \frac{x}{a}) \cos(\lambda_m \frac{y}{l})[1 - e^{-k_{nm}t}] + T_o. \tag{47}$$

A representative result is shown in figure 6. Typically, about five double summations in equation (47) are enough to ensure good convergence of the series.

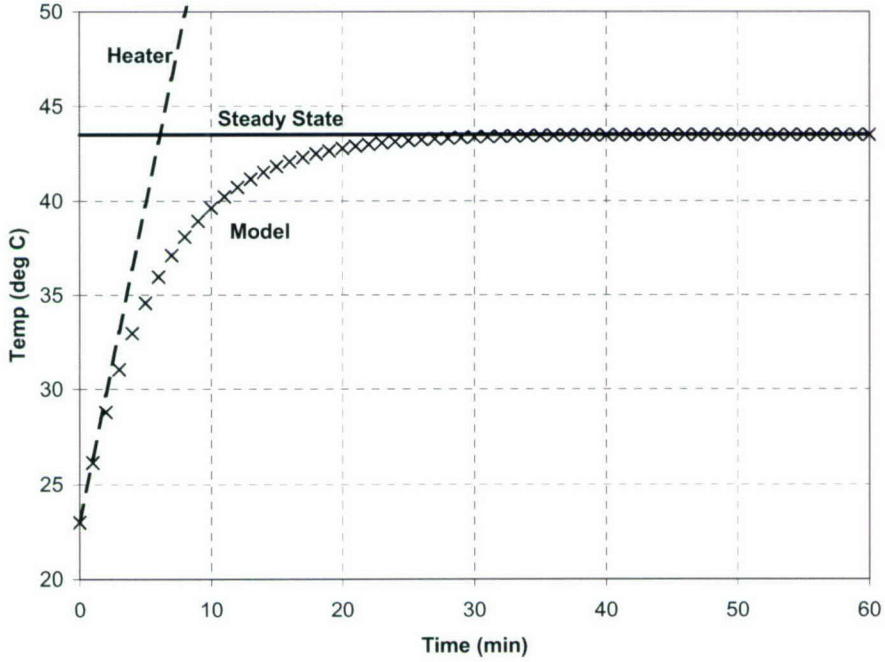

Figure 6. Temperature Response Profile of a Ceramic Cylinder: Analytical Model, Heater, and Steady-State Conditions

4.1 EARLY TIME BEHAVIOR

The initial rate of temperature increase is described by equation (26). If a uniform initial temperature distribution is assumed, then the diffusion term is dropped and equation (26) becomes

$$\frac{\partial T}{\partial t}\Big|_{t=0} = \frac{Q}{\rho C}. \tag{48}$$

The early time behavior of temperature is expressed as

$$T = \frac{Q}{\rho C} t + T_o. \tag{49}$$

It is clear from the internal heat source, equations (31) and (49), that the initial slope of the temperature profile is proportional to the frequency, square of the applied voltage, dielectric constant, and loss tangent, and it is inversely proportional to the specific heat C and wall thickness. This rate of heat generation in the ceramic is that caused by dielectric losses. This portion of this curve is referred to as the "heater." If the ceramic material were perfectly insulated, the temperature would continuously rise along this straight line until catastrophic failure occurred, as shown in figure 6.

4.2 STEADY STATE

The steady-state solution can be obtained directly from equation (47) as the bracketed exponential function approaches 1 and is expressed by

$$T^{ss} = \sum_{nm} A_{nm} \cos(\lambda_n \frac{x}{a}) \cos(\lambda_m \frac{y}{l}) + T_0. \tag{50}$$

The form of this solution, however, does not easily reveal the dependence on the physical parameters of the problem. An approximate expression that more explicitly displays the physics of the problem can be derived by assuming that the length of the cylinder is much larger than the wall thickness. In other words, the diffusion takes place primarily radially through the cylindrical wall of the ceramic.

The energy balance, equation (26), may then be written for steady state with equation (27):

$$k \frac{\partial^2 T}{\partial x^2} + Q = 0. \tag{51}$$

Integrating equation (51) and applying the boundary condition of equation (42) at the fluid interface yields

$$T^{ss}(x) = \frac{Q}{2k} (a^2 - x^2 + \frac{2ak}{h}). \tag{52}$$

At $x = a$, equation (52) becomes

$$T^{ss} = \frac{QV_c}{A_c} \left(\frac{a}{k_c} + \frac{1}{h} \right) + T_0, \tag{53}$$

where V_c is the total volume, A_c is total surface area (including inner diameter (ID), outer diameter (OD), and end surfaces), k_c is thermal conductivity, and a is one-half the wall thickness of the ceramic cylinder. This expression is an approximate expression of the steady-state temperature at the ceramic wall outer surface.

4.3 APPROXIMATE TIME-DEPENDENT MODEL

Spatially averaging the energy balance equations (26) through (30) over the volume of the ceramic yields

$$\frac{\partial \overline{T}}{\partial t} = \frac{Q}{\rho C} - \frac{hA_c}{\rho C V_c}\left(\overline{T} - T_\infty\right). \tag{54}$$

The solution to equation (54) yields the approximate model as follows:

$$\overline{T} = (T^{ss} - T_o)\,(1 - e^{-t/\tau}) + T_0, \tag{55}$$

where the time constant to reach steady state is τ; that is,

$$\tau = \frac{\rho C V_c}{h\, A_c}. \tag{56}$$

Substitution of equation (53) into equation (56) yields the desired expression for temperature in terms of physical parameters:

$$T(t) = \frac{Q V_c}{A_c}\left(\frac{a}{k} + \frac{1}{h}\right)\left(1 - e^{\frac{-t}{\tau}}\right) + T_0. \tag{57}$$

This approximate model is in good agreement with the exact model of equation (47) (see figure 7, which also shows an FE solution for the same problem). The FE solution was calculated by the FLUX2D model shown in figure 8, which also provides the model inputs (reference 13). The agreement between models is reasonably good.

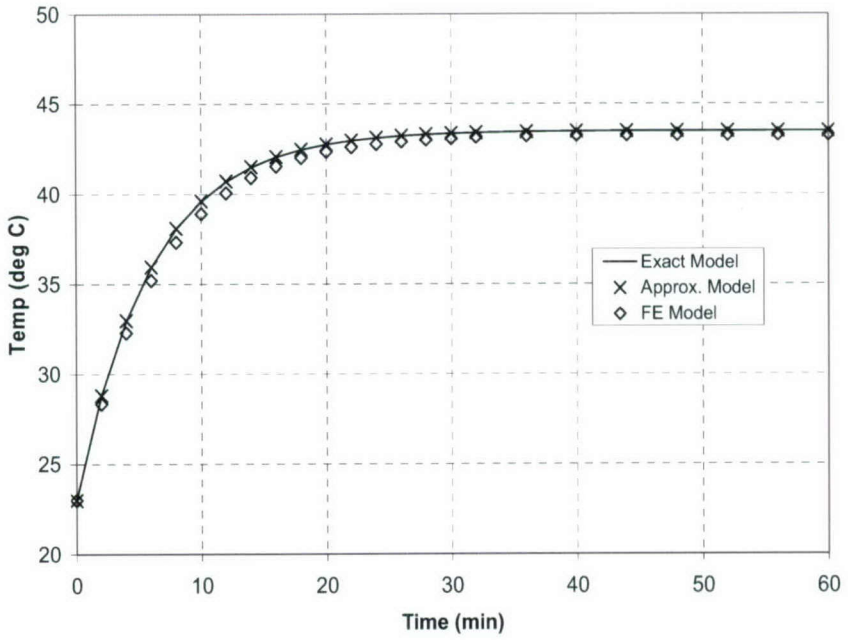

Figure 7. Comparison of Exact Analytical, Approximate, and Axisymmetric FE Model Solutions for Uncoated PZT-8 Ceramic Cylinder with Dimensions of OD = 1.826 Inches, ID = 1.45 Inches, and Length = 0.807 Inch (T_o = 23 ℃)

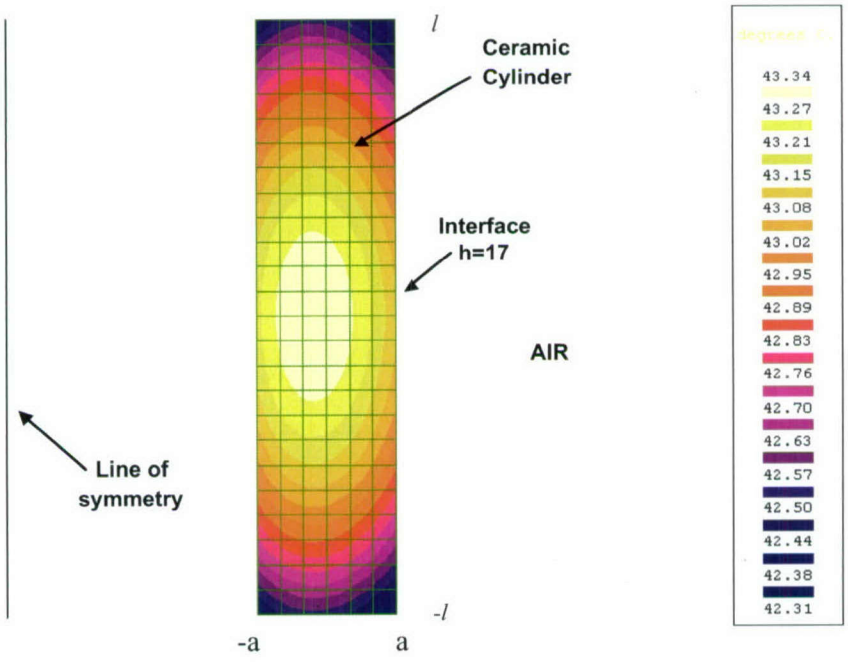

Figure 8. Axisymmetric FE (FLUX2D) Model for PZT-8 Ceramic Cylinder 2 (See Table 2) with Dimensions of OD = 1.826 Inches, ID = 1.45 Inches, and Length = 0.807 Inch at Steady State, Driven at 1000 Vrms (Inputs to Model: f = 10 kHz, h = 17, K^T = 1100, T_o = 23 ℃, Dissipation = 0.0065, k = 2.1, C_c = 420, ρ_c = 7600)

The approximate model shows that to minimize heating, the ratio τ / T^{ss} should be maximized; that is, τ should be large and T^{ss} should be small. This ratio can be written as

$$\tau / T^{ss} = \rho C / Q \frac{(a+l)}{a^2 l}, \tag{58}$$

which implies that a tall, thin cylinder will dissipate the generated heat more efficiently than will a short thick cylinder.

5. MODELS FOR COATED CYLINDERS

A more practical case is a ceramic cylinder encased in a protective polymer coating and driven at high power in a free-field fluid environment. The thermal conductivity and specific heat of coatings are usually less than those of the ceramic; therefore, the ceramic temperature will be nearly uniform throughout its volume at any given instant. This study treats the ceramic and the coating as lumped parameters. A linear temperature profile in the polymer is assumed. FE models (discussed in section 7) indicate that the profile is very linear. The thermal energy balance equation for the coated ceramic may be written as

$$\rho_c C_c V_c \frac{\partial T_a}{\partial t} = Q V_c - k_p A_c \frac{(T_a - T_b)}{d}. \tag{59}$$

The thickness of the coating is d. The temperature subscript a refers to the ceramic/polymer coating interface, and subscript b refers to the polymer coating/fluid interface (see figure 9).

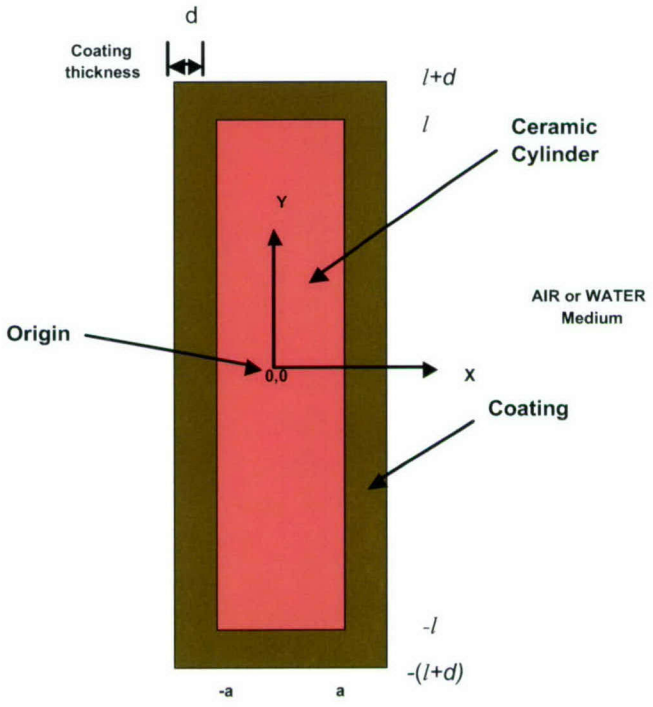

Figure 9. Epoxy-Coated Ceramic Cylinder Layout

The left side of equation (59) is the total rate of change of internal energy in the ceramic (equation (30)). On the right side of equation (59) is the sum of the total rate of internal heat generation plus the total heat flux between the ceramic and coating due to conduction.

In the polymer coating, the energy balance equation is expressed as

$$\frac{1}{2} V_p \rho_p C_p \frac{\partial (T_a + T_b)}{\partial t} = A_p k_p \frac{(T_a - T_b)}{d} - A_p h (T_b - T_\infty). \tag{60}$$

The term on the left of equation (60) represents the total rate of change in internal energy for the coating. The average temperature of the coating is represented by the algebraic sum of the temperature at the ceramic surface and the temperature at the coating/fluid interface. On the right side of equation (60), the first term is the rate of heat flow between the coating and ceramic, (equation (28)), and the second term is the rate of convective flow into the fluid (equation (29)).

Differentiating equations (59) and (60) with respect to time can decouple these two equations, the details of which are presented in appendix A. Equation (61), which is the same as that in equation (A-10), represents the thermal energy balance of the system in terms of the temperature at the ceramic/polymer coating interface:

$$\frac{\partial^2 T_a}{\partial t^2} + \varepsilon_1 \frac{\partial T_a}{\partial t} + \varepsilon_2 T_a = \varepsilon_3 Q_c, \tag{61}$$

with

$$\varepsilon_1 = 2 \tau_c + \tau_p + \tau_h; \quad \varepsilon_2 = \tau_c \tau_h; \quad \varepsilon_3 = \tau_p + \tau_h, \tag{62}$$

and defining

$$Q_c \equiv \frac{Q}{\rho_c C_c}; \tau_c \equiv \frac{k_p A_c}{d \rho_c C_c V_c}; \tau_p \equiv \frac{2 k_p A_p}{d \rho_p C_p V_p}; \tau_h \equiv \frac{2 h A_p}{\rho_p C_p V_p}. \tag{63}$$

Here, the piezoelectric ceramic material and polymer coating material are represented by the subscripts c and p, respectively. The V's and A's are the volumes and areas, respectively, of the ceramic and coating (only the area exposed to the fluid in the case of the coating). These parameters have units of inverse time. Their inverses represent characteristic thermal relaxation times for conduction or convection. For example, $1/\tau_c$ is a measure of the relaxation time for conduction of heat from the ceramic to the coating.

The solution to equation (61) may be expressed in the form

$$T_a = \frac{Q}{\tau_s \ \rho_c \ C_c} + A e^{\lambda_1 t} + B e^{\lambda_2 t}, \tag{64}$$

where

$$\tau_s = \frac{\varepsilon_2}{\varepsilon_3 \varepsilon_1}, \tag{65}$$

and

$$\lambda_{1,2} = -\frac{1}{2} \ \varepsilon_1 \left(1 \pm \sqrt{1 - 4 \ \frac{\varepsilon_2}{\varepsilon_1}} \right). \tag{66}$$

The plus sign in equation (66) refers to λ_1, and the minus sign refers to λ_2. The λ's, as was the case for the τ's, also have units of inverse time. They are decay constants for the overall system; that is, their inverses are characteristic relaxation times for the complete system. They determine the rate at which the steady-state temperature is reached.

The temperature at the polymer/fluid interface may now be found from either equation (59) or (60) as

$$T_b = \left(\frac{1}{\tau_s} - \frac{1}{\tau_c}\right) \frac{Q}{\rho_c \ C_c} + \left(1 + \frac{\lambda_1}{\tau_c}\right) A e^{\lambda_1 t} + \left(1 + \frac{\lambda_2}{\tau_c}\right) B e^{\lambda_2 t}. \tag{67}$$

Using the initial condition that the temperatures are uniform and the same in both the ceramic, coating, and the fluid, constants A and B can be evaluated by setting $t = 0$ in equations (64) and (67) and substituting the initial conditions $T_a = T_b = T_0$ to obtain these results:

$$A = \tau_s \frac{Q}{\rho_c C_c} \frac{(\lambda_2 + 1)}{(\lambda_1 - \lambda_2)}, \tag{68}$$

$$B = -\tau_s \frac{Q}{\rho_c C_c} \frac{(\lambda_1 + 1)}{(\lambda_1 - \lambda_2)}. \tag{69}$$

6. ASYMPTOTIC LIMITS AND APPROXIMATE SOLUTIONS FOR COATED CYLINDERS

An examination of the initial time behavior and the steady-state behavior provides a means of verifying the solutions for coated cylinders. Moreover, the solution is simplified, so that the influence of the physical parameters is more apparent.

6.1 INITIAL TIME BEHAVIOR

Let t approach zero in equation (59) and integrate with respect to time. Then, by applying the initial conditions that $T_a = T_b = T_0$ at $t = 0$ and assuming a uniform temperature distribution, the same expression is obtained as before for the heater (equation (49)); namely,

$$T_a = \left(\frac{Q}{\rho_c C_c}\right) t + T_0 \quad \text{as } t \rightarrow 0, \tag{70}$$

which is in agreement with the result expected from assuming a uniform temperature and integrating equation (26). If the ceramic was perfectly insulated, the temperature would rise linearly versus time, that is, the heater portion of the temperature curve, as discussed in section 4.

6.2 STEADY STATE

By letting t approach infinity (∞) in equations (59) or (60), the steady-state temperature can be found by integrating with respect to time and applying the boundary condition at the interface. Assuming $A_P \approx A_c$, at $x = a$,

$$T_a^{ss} = \left(\frac{1}{h} + \frac{d}{k_p}\right) \frac{V_c Q}{A_c} + T_0, \tag{71}$$

where d is the thickness of the coating, and k_p is the thermal conductivity of the coating material.

If equation (71) is written as

$$T_a^{ss} - T_0 = \left(\frac{1}{h} + \frac{d}{k_p}\right) \frac{V_c Q}{A_c}, \tag{72}$$

it can be seen that, for a given volume-to-area ratio and a given heat source Q, the controlling parameters are $1/h$ and d/k_P. If h is very large, as is the case for water where h is on the order of 100 or greater, the steady state is determined by the thickness-to-conductivity ratio $\left(d/k_p\right)$. If, as is the case for air, h is relatively small, then the convection process dominates. When the

length of the ceramic is much greater than its wall thickness, $V_c/A_c \approx a$, equation (72) can be approximated as

$$T_a^{ss} - T_0 = \left(\frac{1}{h} + \frac{d}{k_p}\right) a\, Q, \tag{73}$$

which illustrates a linear dependence of the steady-state condition on the thickness of the ceramic.

6.3. SIMPLIFIED SOLUTIONS

The general solution for a coated cylinder, equation (67), contains two time constants, λ_1 and λ_2. In most instances, these differ by several orders of magnitude. Thus, one component vanishes very early in time relative to the longer-lived component. Equation (64) may thus be rewritten as

$$T_a = \frac{Q}{\tau_s\ \rho_c\ C_c} + B e^{\lambda_2 t}\left[1 + \frac{A}{B} e^{(\lambda_1 - \lambda_2)t}\right] + T_0, \tag{74}$$

or, substituting equations (68) and (69),

$$T_a = \frac{Q}{\tau_s\ \rho_c\ C_c} + B e^{\lambda_2 t}\left[1 - \frac{\lambda_2 + 1}{\lambda_1 + 1} e^{(\lambda_1 - \lambda_2)t}\right] + T_0. \tag{75}$$

Both time constants are negative (as they should be physically), but one can see from equation (66) that $|\lambda_1| >> |\lambda_2|$. Thus, the solution can be approximated as

$$T_a = T_0 + \frac{Q}{\tau_s\ \rho_c\ C_c} + B e^{\lambda_2 t}. \tag{76}$$

Using equation (69) yields

$$T_a = \frac{Q}{\tau_s\ \rho_c\ C_c}\left[1 - \tau_s^2\left(\frac{\lambda_1 + 1}{\lambda_1 - \lambda_2}\right) e^{\lambda_1 t}\right] + T_0. \tag{77}$$

Recall that at initial time $t = 0$, $T_a = T_0$, which implies that

$$\tau_s^2\left(\frac{\lambda_1 + 1}{\lambda_1 - \lambda_2}\right) \approx 1 \tag{78}$$

in equation (75) and, thus,

$$T_a \approx \frac{Q}{\tau_s \ \rho_c \ C_c} (1 - e^{\lambda_2 t}) + T_0. \tag{79}$$

Figure 10 compares the simplified model (equation (79)) with the more exact result obtained with equation (64). The temperature profile computed with a FLUX2D FE model is included in figure 10 and is also shown in figure 11 (model inputs are also included in figure 11).

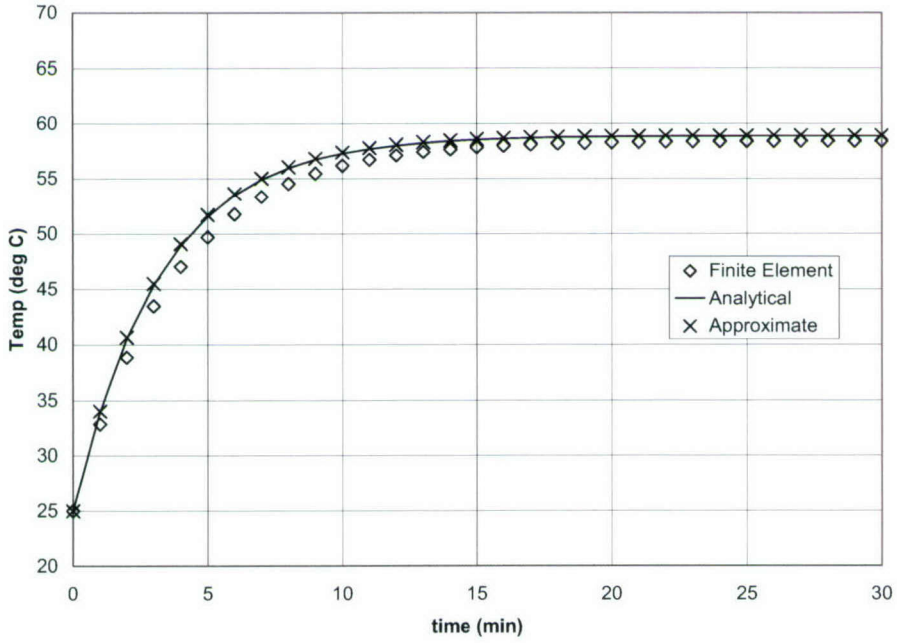

Figure 10. Comparison of Exact Analytical Solution and Approximate Solution for Coated PZT-8 Ceramic Cylinder 3 (See Table 2) with Dimensions of OD = 1.054 Inches, ID = 0.791 Inch, and Length = 0.527 Inch (T_o = 25°C)

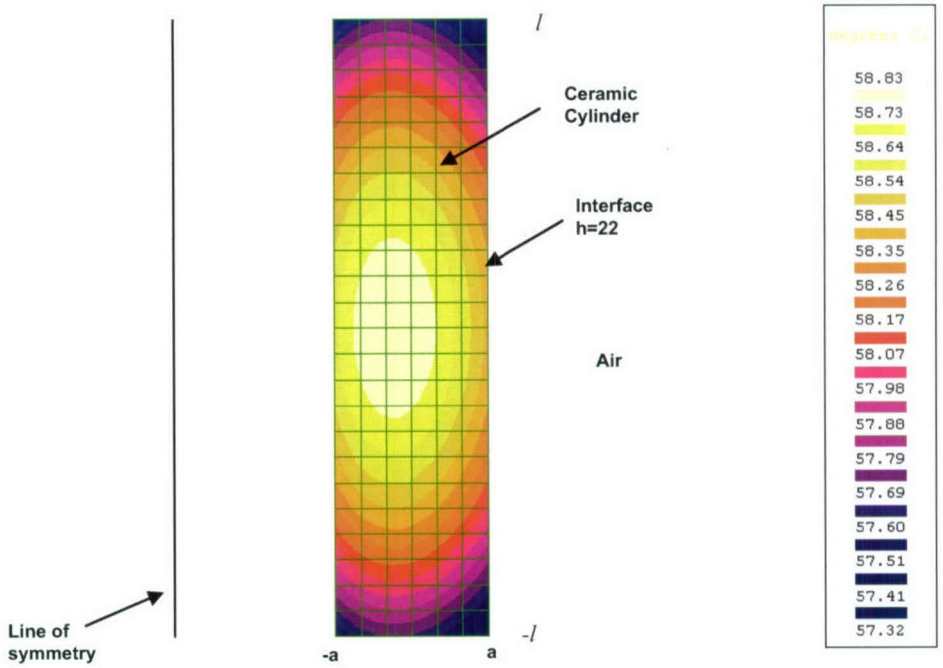

Figure 11. Axisymmetric FE (FLUX2D) Model for Coated PZT-8 Ceramic Cylinder 3 (See Table 2) with Dimensions of OD = 1.054 Inches, ID = 0.791 Inch, and Length = 0.527 Inch at Steady State, Driven at 1000 Vrms (Input to Models: f = 10 kHz, h = 22, K^T = 1100, T_o = 25 ℃, Dissipation = 0.01, k = 2.1, C_c = 420, ρ_c = 7600)

7. MEASUREMENT VERSUS MODEL

7.1 BARE CYLINDERS IN AIR

The first thermal tests were conducted on bare cylinders in air. The temperature was measured by a thermocouple attached to the outer radius of the cylinder at the midpoint of the length (see figure 12). Two important quantities were the (1) temperature-versus-time profile of the outer surface, and (2) temperature at the region midway between the inner and outer surfaces. The center region is expected to be the hottest, but there is no practical way to measure the temperature. The models developed in section 4 were used for comparison. (The models are analytical models (that is, closed-form equations), but some finite element analyses (FEA) were also used to verify the models and the data.)

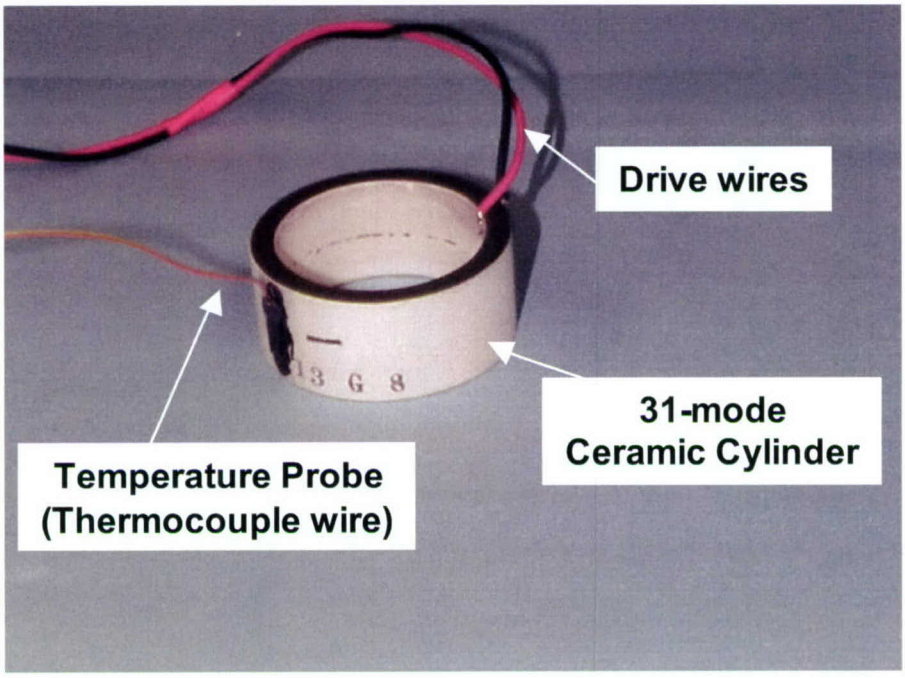

Figure 12. Uncoated Ceramic 31-Mode Cylinder with Thermocouple Wire Epoxied

Three cylinders with different dimensions (see table 2) and properties (see table 3) were modeled. These cylinders were suspended in air by their drive wires in an enclosure to reduce air currents. Note that one cylinder was composed of PZT-4 (Navy Type I) material and the others of PZT-8 (Navy Type III) material. Each cylinder was driven at three voltage levels (500, 750, and 1000 Vrms) below their first resonance while their electrical input current, phase, and power were monitored. The modeling results for these three cylinders are shown in figures 13, 14, and 15.

Table 2. Piezoelectric Ceramic Cylinder Dimensions and Measured Small Signal Properties

Cylinder No.	OD (in./cm)	ID (in./cm)	Length (in./cm)	Material	Resonant Frequency (kHz)	k_{eff}	Cap (nF)	Diss ($\tan\delta_e$)
1	2.546/ 6.467	2.160/ 5.486	0.964/ 2.449	PZT-4 (Type I)	17.2	0.34	10.8	0.0032
2	1.826/ 4.638	1.454/ 3.693	0.807/ 2.050	PZT-8 (Type III)	26.2	0.33	5.5	0.0026
3	1.054/ 2.677	0.791/ 2.009	0.527/ 1.339	PZT-8 (Type III)	47.1	0.32	2.5	0.0034

Table 3. Piezoelectric Ceramic Material Properties (References 7 – 10)

Property	PZT-4 (Navy Type I)	PZT-8 (Navy Type III)
Density ρ (kg/m^3)	7600	7600
Curie Temperature (°C)	≥300	≥300
Heat Capacity C_c (J/kg °C)	420	420
Thermal Conductivity k_c (W/m °C)	2.1	2.1
Dielectric Constant K^T ($\varepsilon^1/\varepsilon_0$)	1300	1000 – 1100
Dissipation Factor ($\tan\delta$) Large Signal (4 kVrms/cm)	0.04	0.01

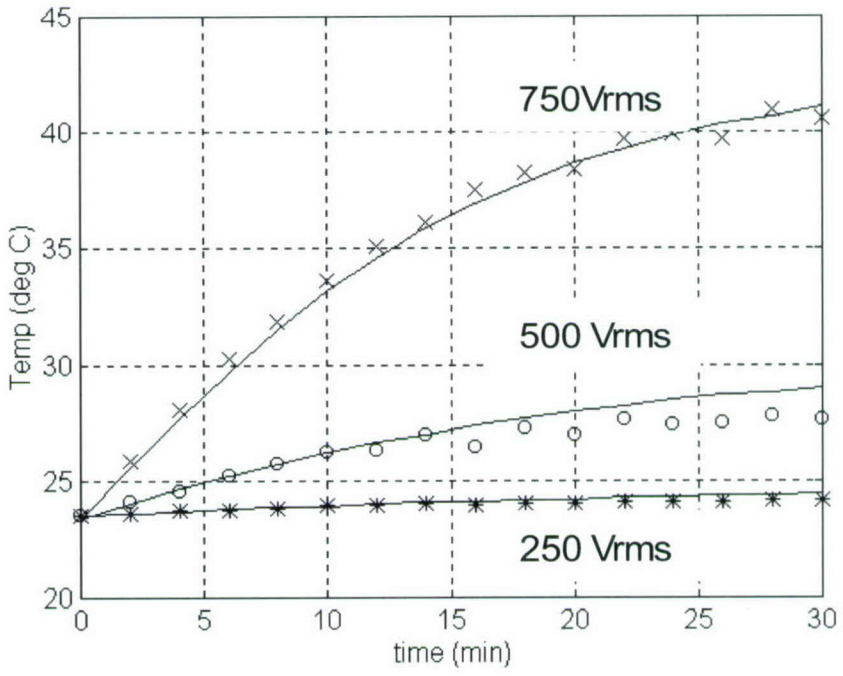

*Figure 13. Modeled (+, o, *) and Measured (—) Uncoated Cylinder 1 In-Air Results at 5 kHz*

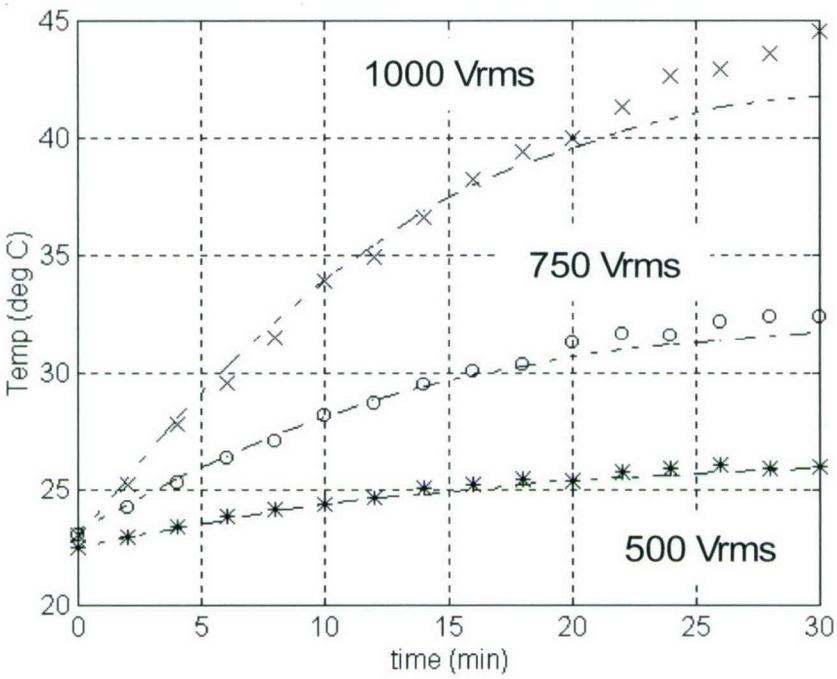

Figure 14. Modeled (+, o, *) and Measured (------) Uncoated Cylinder 2 In-Air Results at 10 kHz

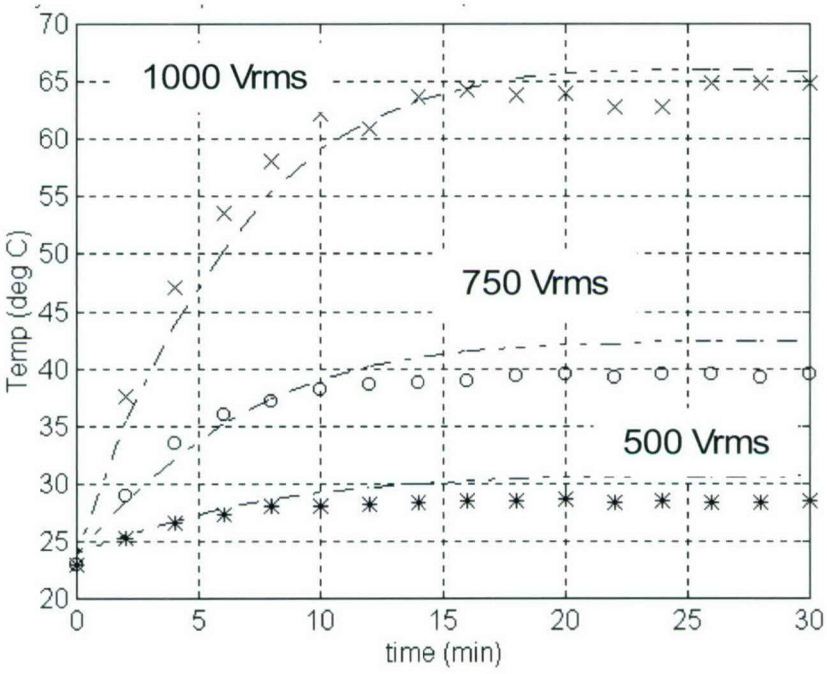

Figure 15. Modeled (+, o, *) and Measured (------) Uncoated Cylinder 3 In-Air Results at 10 kHz

The modeled rate of internal heat generation per unit volume was assumed equal to the full measured input wattage at each measured temperature. To validate this assumption, the internal heat generated was also computed from equation (31) using measured values of dissipation and dielectric constants (see appendix B). Note that measured values were used because the "book values" (references 7 – 10) for permittivity and dissipation did not correspond to measured values. In each case, both sources produced identical time-temperature curves. Note that the curves generated by the model are not smooth—caused by a non-smooth variation in the dissipation curves in appendix B. This variation in the dissipation may be attributed to measurement error resulting from the measured quantities being near the resolution limits of the instrument. The dielectric constant also varies with temperature, but quite smoothly. The measured electrical input power, dielectric constant, and dielectric dissipation factor for each cylinder are shown in appendix B. A measured example of a cylinder in thermal runaway leading to fracture of the cylinder is shown in figure 16.

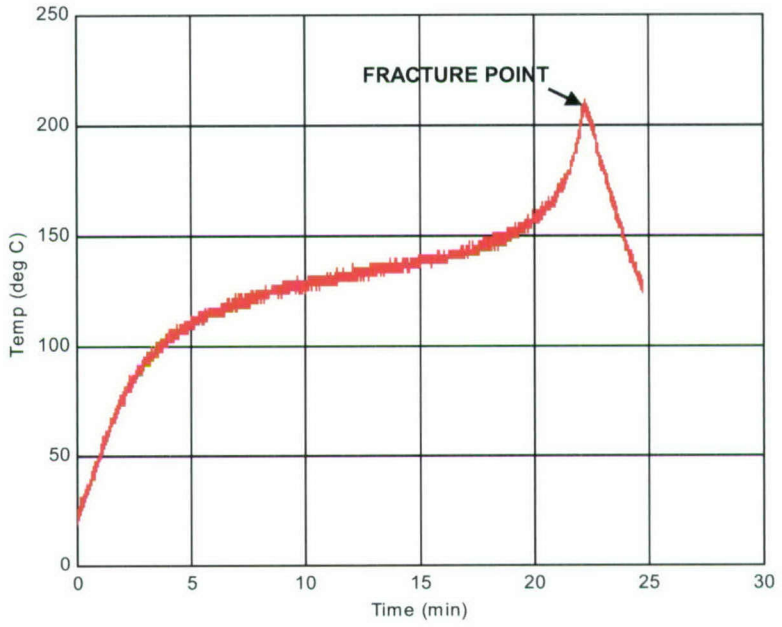

Figure 16. Measured Example of a Cylinder in Thermal Runaway Leading to Fracture of the Cylinder

Variations in the film coefficient h show a consistent pattern: they decrease with cylinder size and increase with frequency (see table 4). For engineering purposes, the film coefficient depends primarily on the inverse of the boundary layer thickness (reference 11). Thus, it is reasonable to see a variation of h with cylinder size; however, the dependence on frequency is difficult to explain. An in-depth analysis of the film coefficient is beyond the scope of this report, but the values of h used are in the range of values used in engineering calculations for the convection of air over smooth surfaces (reference 14) (see table 5). Choosing h in water was conveyed via private communication with a heat transfer specialist (reference 15).

Table 4. In-Air Convection Film Coefficients (h) for Different Ceramic Cylinders

Cylinder No.	5 kHz	10 kHz	15 kHz
1	10	--	--
2	--	17	22
3	--	22	30

Table 5. Representative Values of Convective Heat Transfer Coefficients (Approximate)

Type of Convection: Fluid	h (W/m^2 °C)
Free, Air	5 – 25
Forced, Air	10 – 500
Forced, Water	100 – 15,000
Forced, Boiling Water	2500 – 25,000
Forced, Condensing Steam	5000 – 100,000

7.2 COATED CYLINDERS IN AIR

The same set of cylinders was coated with an epoxy, and the same set of measurements were taken as those for the uncoated set of cylinders. The applied epoxy has a relatively high thermal conductivity ($k \approx 1$) and high heat capacity ($C \approx 1400$), but a low electrical conductivity. Thus, the epoxy was expected to provide adequate water barrier, electrical insulation, and good thermal properties for the removal of heat from the ceramic core, which is vitally important for high-power drive in water. Polyurethane and epoxy coating material properties are given in table 6. Figure 17 shows a representative coated cylinder (figure 9 in section 5 presents the layout used to model this case). Measurements were compared with results using equation (64) in figures 18 through 20. The values of h assumed in the model were the same as those used for the bare cylinders (see table 4). For each cylinder, at each drive level tested, the analytical model predicts the measured temperature rise.

Table 6. Coating Material Properties

Property	Polyurethane	Epoxy
Density (kg/m^3)	1100-1200	1830
Heat Capacity (J/kg °C)	80	1400
Thermal Conductivity (W/m °C)	0.2	1
Sound Speed (m/s) Bulk/Bar	1400-1700/NA	2700/1900

N/A = not applicable.

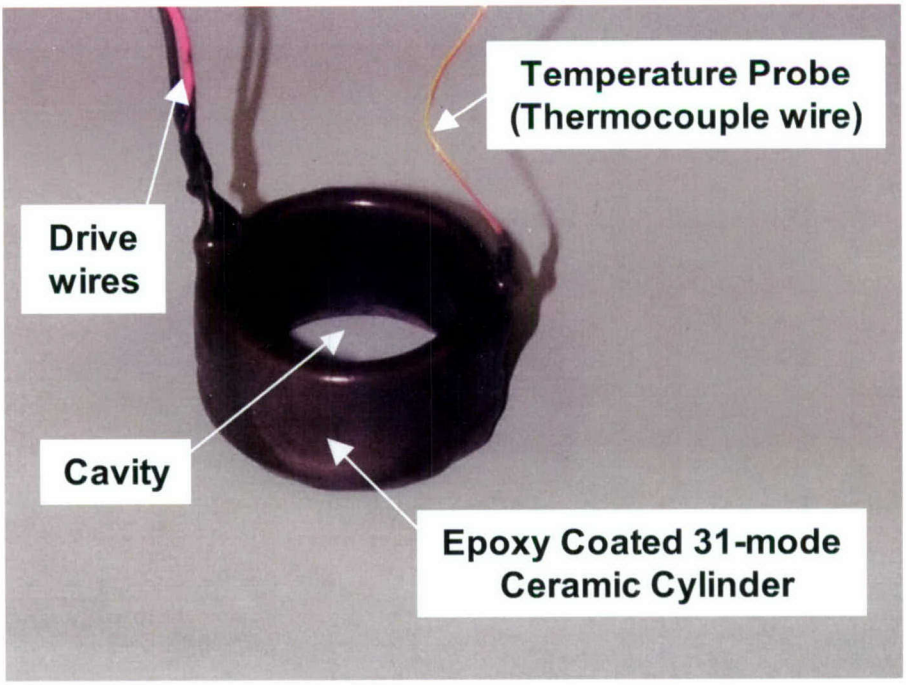

Figure 17. Epoxy-Coated, 31-Mode Ceramic Cylinder with Thermocouple

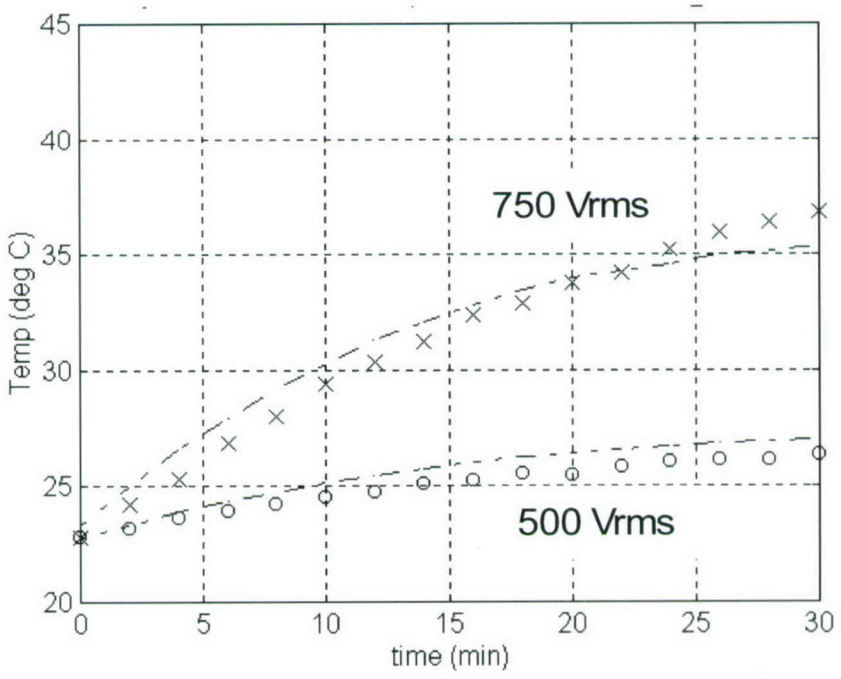

Figure 18. Modeled (+, o) and Measured (------) Coated Cylinder 1 In-Air Results at 5 kHz, Coating Thickness = 0.023 Inch (0.58 mm)

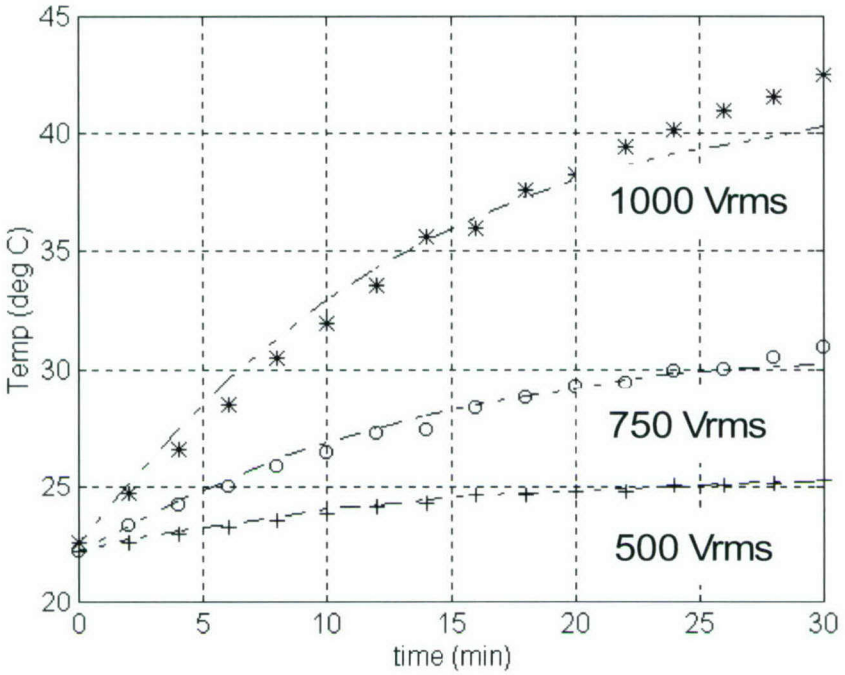

Figure 19. Modeled (+, o, *) and Measured (------) Coated Cylinder 2 In-Air Results at 10 kHz, Coating Thickness = 0.022 Inch (0.56 mm)

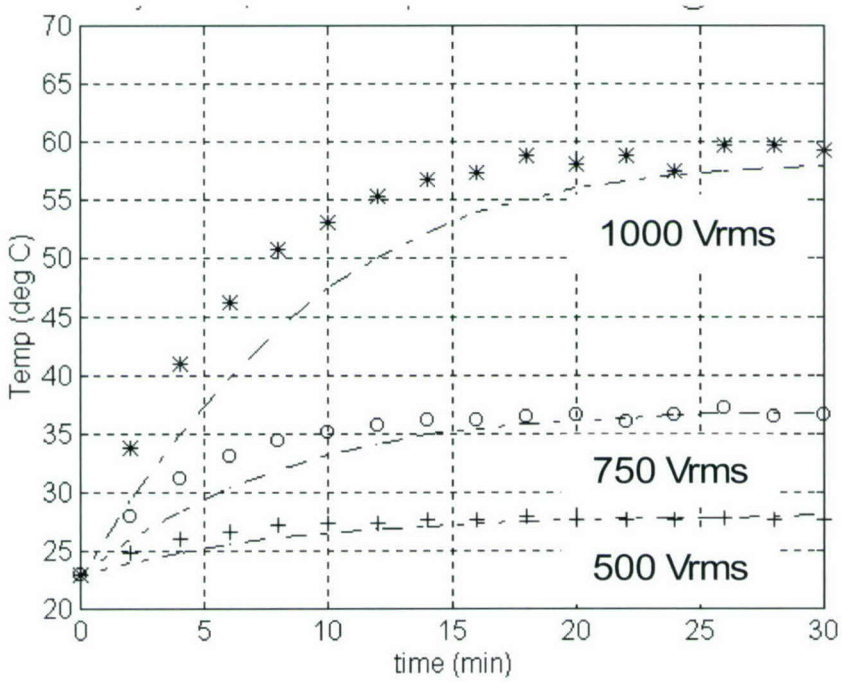

Figure 20. Modeled (+, o, *) and Measured (------) Coated Cylinder 3 In-Air Results at 10 kHz, Coating Thickness = 0.021 Inch (0.54 mm)

7.3 IN-WATER MEASUREMENTS COMPARED WITH MODELS

A thermal life test was conducted on a free-flooded cylinder (cylinder 2) coated in a 0.022-inch-thick layer of a thermal conductive epoxy (E-301AD, manufactured by CASTALL Inc., Weymouth, MA). A 50-foot thermocouple wire (temperature probe) was embedded in the epoxy coating, and the temperature was monitored on a digital temperature meter, as shown in figure 17. Testing was conducted at the Acoustic Pressure Tank Facility (APTF) at the Naval Undersea Warfare Center (NUWC) Division, Newport, RI.

The APTF measurement test vessel is a closed, water-filled steel tank that measures 36.5 feet long by 12.5 feet in diameter and can be pressurized to 2700 psig. The free-flooded cylinder was positioned in the center of the tank, and the hydrophone was positioned at a 4.15-meter distance for monitoring the generated sound pressure level. The tank was pressurized to 50 psig to avoid cavitation that would be generated by the transducer at a high sound pressure level. The cylinder was tested with three different, constant, steady-state drive voltage levels at 26 kHz for 20-minute durations. The cylinder was allowed to cool in the tank to ambient temperature (16.6°C) between changes in drive voltage. The drive voltage levels were 1000 Vrms, 1400 Vrms, and 1750 Vrms, which equate to source levels of 193 dB, 196 dB, and 198 dB re 1 μPa at 1 meter, respectively (see the measured transmit voltage response (TVR) of cylinder 2 plotted in figure 21). As shown in the TVR, a free-flooded cylinder produces a double-resonant transmitting pressure response, where the lower resonance is generated by the inner cavity of the cylinder acting as a Helmholtz resonator, and the upper resonance is caused by the fundamental circumferential cylinder resonance that radiates acoustic energy from both the inner and outer surfaces of the cylinder walls. This cavity resonance is combined with the "ring" resonance to produce a broadbandwidth transmitting response that is depth independent.

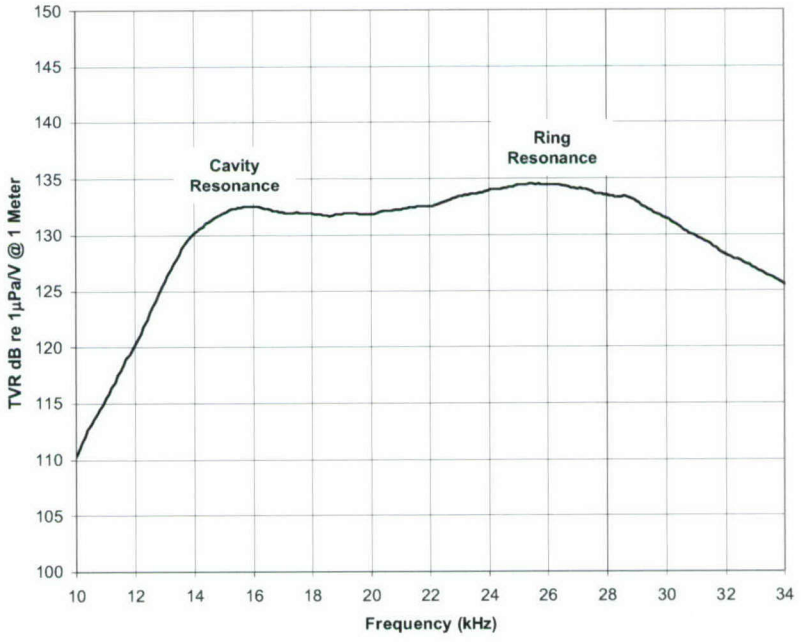

Figure 21. Measured TVR of Cylinder 2

Absolute sound pressure level measurements could not be made in the tank because of reflecting and standing waves caused by the steady-state continuous drive signals that were used. The measured electrical input powers associated with the three different drive voltages are shown in figure 22.

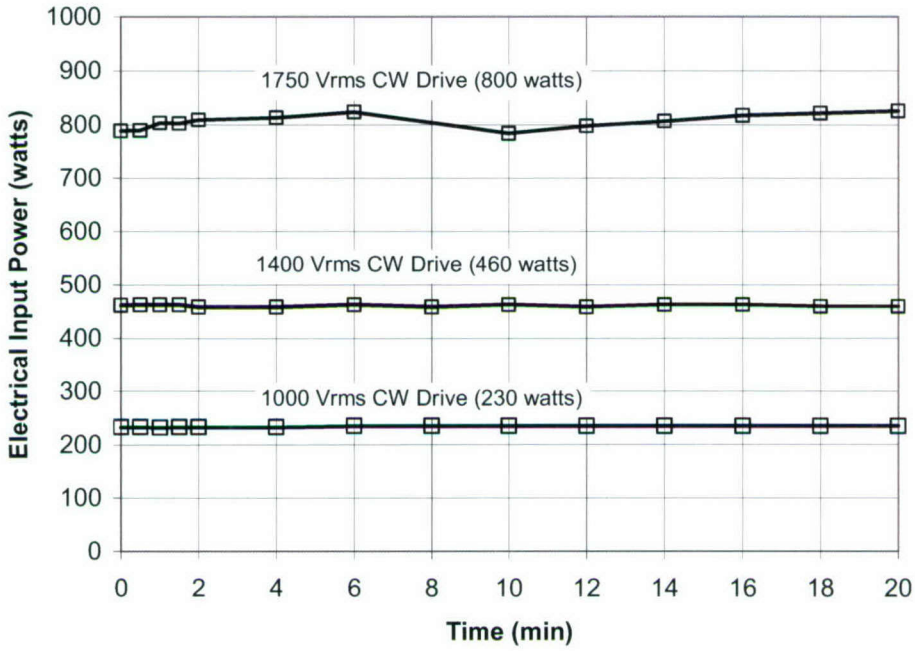

Figure 22. Measured Electrical Input Power Levels of Free-Flooded Test Cylinder for Three Different Steady-State Voltage Drive Levels at 26 kHz (Tank Pressure 50 psig)

The relative flatness of the power responses over time indicate that the impedance magnitude and impedance phase angle of the cylinder remain constant over time and that heat energy generated in the cylinder (caused by the electrical drive power) is dissipated through the epoxy into the surrounding water as fast as it is generated. This finding is evident by the measured, in-water steady-state temperature profile for the different voltage drive levels (see figure 23). The in-water analytical results for coated cylinder 2 is shown in figure 24 for 1400-Vrms drive and a film coefficient of 1350 W/m^2 °C.

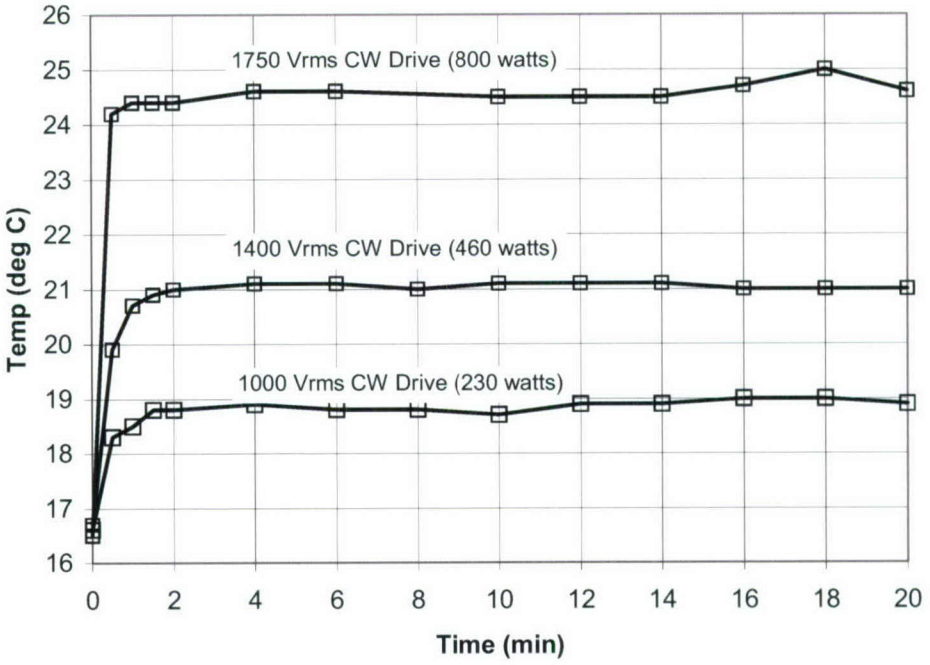

Figure 23. In-Water Measured Cylinder 2 with Epoxy Coating at 26 kHz (Ring Resonance) and 1400-Vrms Drive

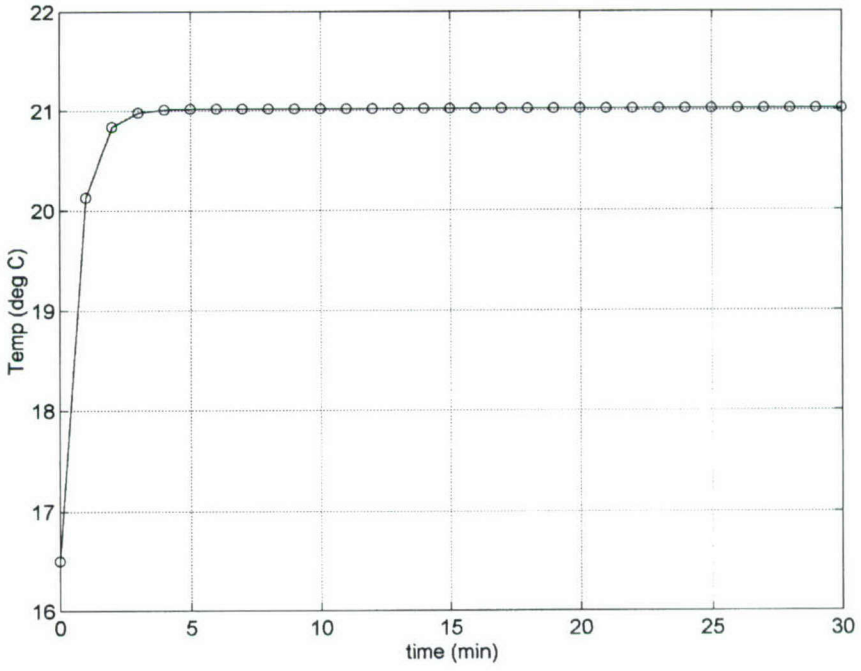

Figure 24. In-Water Analytical Model of Cylinder 2 with Epoxy Coating at 26 kHz (Ring Resonance) and 1400-Vrms Drive

For validation of the simple analytical model and measurements, a coupled electromechanical thermal analysis was performed with the ATILA FE code. In the ATILA code, losses in active and passive materials are accounted for by using complex physical constants for dielectric, mechanical, and piezoelectric properties. The dissipated power for each element and for the whole transducer structure can be obtained (reference 16); a thermal analysis by heat transfer that includes conduction and convection provides the temperature profile in the transducer. For a steady-state solution, thermal behavior is weakly coupled to the electromechanical response. The solution may thus be performed as a two-step analysis, for which the electromechanical behavior is first computed and the resulting dissipated power is then applied as a heat generator to determine the resulting temperature of the system.

Figure 25 compares the measured and computed ATILA-modeled acoustic TVR for cylinder 2. The modeled acoustic performance closely matches the measured response. Figure 26 depicts cylinder 2 with a thermally conductive epoxy coating that was driven in water at the ring resonance. The FE model tracks the steady-state solution temperature. The temperature profile computed at the ring resonance is depicted in figure 27, where a section of the cylinder and epoxy coating is hidden to display the temperature through the cylinder thickness. Note the temperature at equilibrium remains near ambient because of the good volume-to-surface-area ratio for the free-flooded projector. If the temperature rise was significant, however, because material properties are temperature dependent, additional analysis steps would be performed with updated material properties until equilibrium is reached.

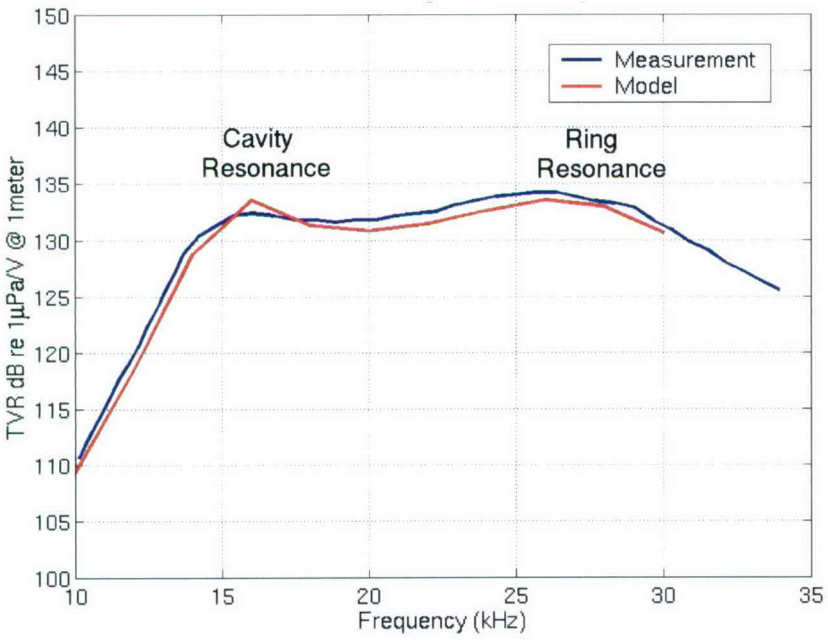

Figure 25. Comparison of Measured and FEA-Modeled (ATILA) Acoustic TVR for Free-Flooded Cylinder 2

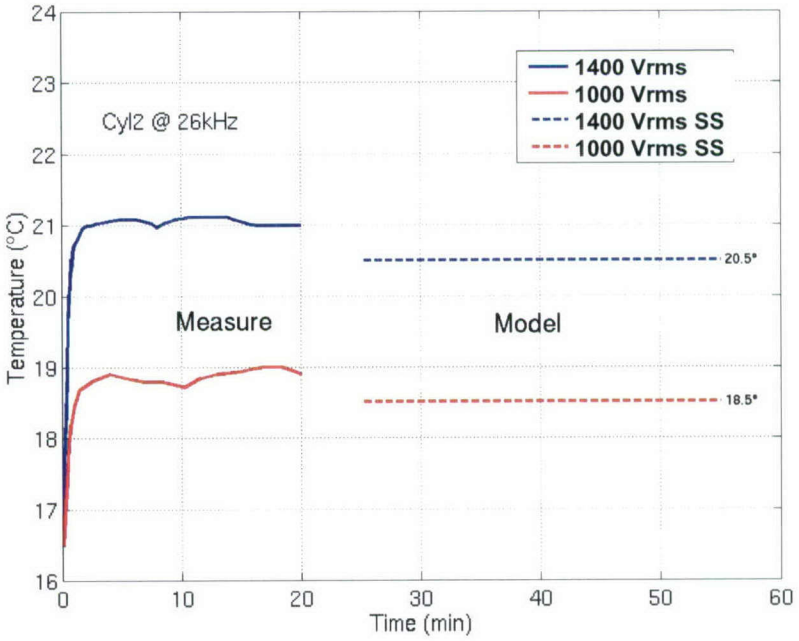

Figure 26. Measured and Steady-State (SS) FEA Model of Free-Flooded Cylinder 2 in Water, Driven at 1000 Vrms and 1400 Vrms at 26 kHz (Ring Resonance)

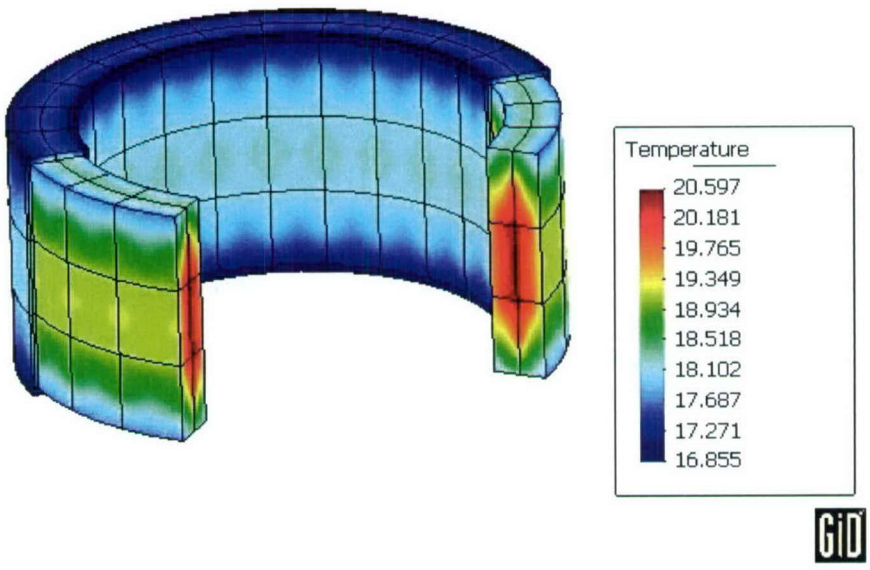

Figure 27. In-Water Steady-State ATILA FEA Model Temperature Profile Through a Section of Cylinder 2, with Epoxy Coating Cut Back, Driven at 1400 Vrms at 26 kHz (Ring Resonance), Coating Thickness d = 0.022 Inch (Inputs to Model: $f = 26$ kHz, $h = 1350$ W/m^2 °C, $K^T = 1100$, $T_o = 16.5$ °C, Dissipation = 0.01, $k = 2.1$, $C_c = 420$, $\rho_c = 7600$)

7.4 COMPARISON OF COATINGS

The analytical model represented by equation (61) is based on the assumptions that the temperature in the ceramic is uniform and that the temperature varies linearly in the coating. To verify this assumption, an FE model was used to calculate the temperature profiles through the cross section of the ceramic and epoxy and polyurethane coatings. Figure 28 shows the in-air steady-state solution for the FE model calculated with both the high thermal conductivity epoxy coating used in the measurements and a lower thermal conductivity polyurethane. The results of this FE model demonstrate that the assumptions are reasonable.

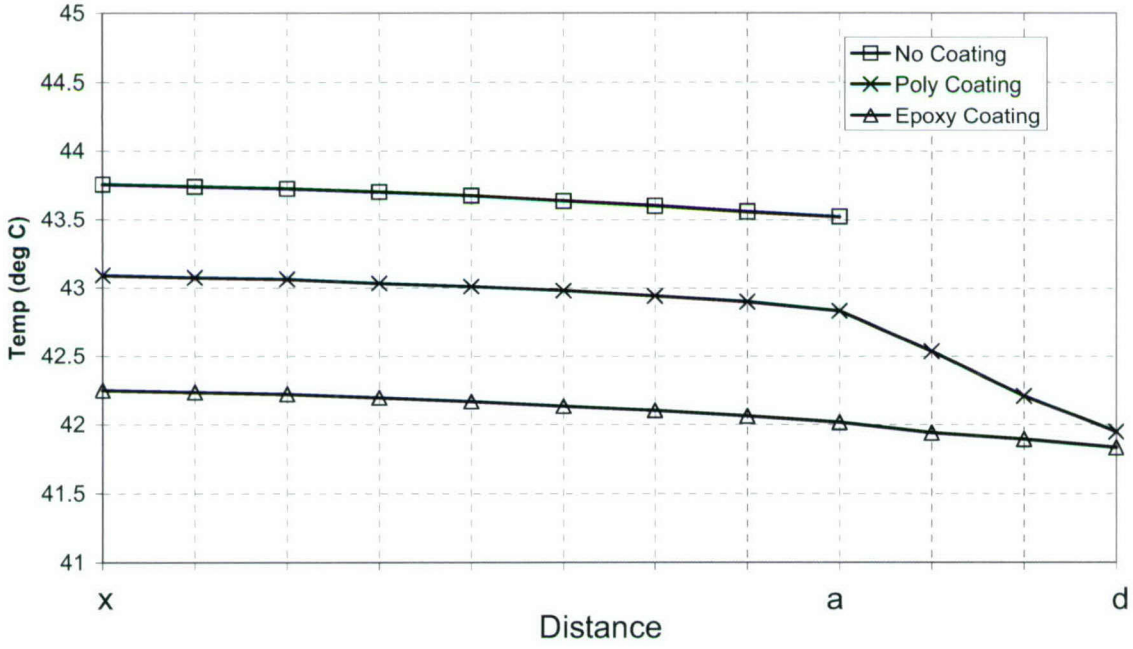

Figure 28. In-Air FE Temperature Contour of Cylinder 2 from Center of Cylinder x to Outer Layer of Coating d with and without Coating, Driven at 1000 Vrms (a = Outer Radius of Cylinder, T_o = 23 °C), Coating Thickness d = 0.022 Inch (Inputs to Model: f = 10 kHz, h = 17 W/m^2 °C, K^T = 1100, T_o = 23 °C, Dissipation = 0.01, k = 2.1, C_c = 420, ρ_c = 7600)

Comparing the results for the coated cylinders with those for the uncoated cylinders reveals that the temperature profiles are about the same for these thin coatings. This result is a consequence of an earlier observation (in section 6.2) that when the $1/h$ term dominates (h small) over the d/k_p term, the heating process is dominated by convection. In the case of holding the convection coefficient constant, the high conductivity coating will draw heat away from the ceramic cylinder (that is, it will act as a heat sink).

For comparison, in-water FE models were used to calculate the steady-state temperature profiles in the coatings as the thickness was increased to 0.2 inch, which is typical of a commercially available free-flooded ring transducer coated with polyurethane. Figure 29 shows the results for an ambient water temperature of 20°C of cylinder 2 driven at 1000 Vrms. The

results show that the polyurethane diverges at a much greater slope than does the epoxy coating when compared to a non-coated case. The epoxy coating thickness can be significantly thinner than the polyurethane coating because it is a tougher material. Comparing the epoxy coating thickness of 0.0625 inch with polyurethane coating thickness of 0.2 inch, the polyurethane temperature is 30°C higher. If the water temperature was 40°C, as encountered in various ocean environments, and the drive voltage of the cylinder was 1750 Vrms (as in section 7.3), the polyurethane-coated cylinder would reach a temperature of 138°C (close to one-half the Curie temperature of PZT) and an epoxy-coated cylinder would reach a temperature of 50°C for a 0.0625-inch thickness or 63°C for a 0.2-inch thickness.

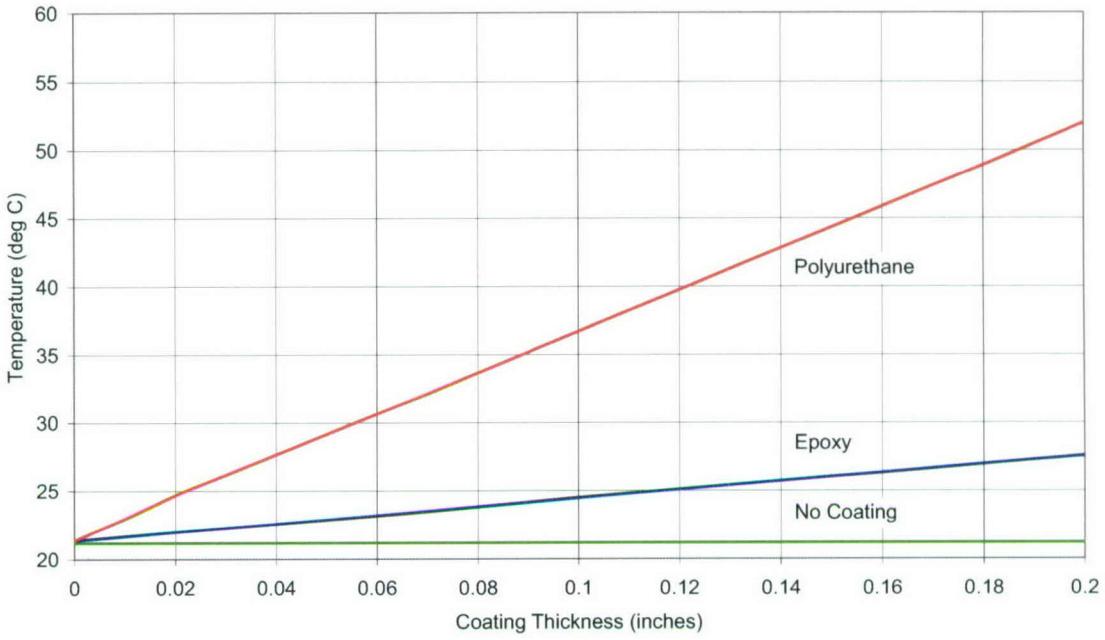

Figure 29. In-Water FE Steady-State Temperature Profile of Cylinder 2 as Thickness of Epoxy and Polyurethane Coatings Is Increased (Inputs to Model: $f = 26$ kHz, $h = 1350$, $K^T = 1100$, $T_o = 20$ °C, Dissipation = 0.01, $k = 2.1$, $C_c = 420$, $\rho_c = 7600$)

Table 7 shows the FE model calculated temperatures for different coating thicknesses and different drive levels for the epoxy and polyurethane coatings. Note that the temperature increase with drive level is linear with the voltage squared (or electric field), as in equation (31).

Table 7. FE Model Calculated Steady-State Temperature for Different Coating Thickness (Inputs to Model: $f = 26$ kHz, $h = 1350$, $K^T = 1100$, $T_o = 0$ °C, Dissipation = 0.01, $k = 2.1$, $C_c = 420$, $\rho_c = 7600$)

Coating Thickness (inch)	Temperature (°C)					
	Epoxy			Polyurethane		
	1000 Vrms	1400 Vrms	1750 Vrms	1000 Vrms	1400 Vrms	1750 Vrms
0.0	1.4	2.7	4.1	1.4	2.7	4.1
0.22	2.0	4.0	5.9	5.0	9.9	15.9
0.0625	3.3	6.5	10.2	11.0	23.7	36.9
0.2	7.6	14.9	23.3	32.0	62.7	98.0

Figure 30 compares the in-water temperature profiles of the two coatings different thermal properties. The epoxy coating has a high thermal conductivity and heat capacity; the polyurethane coating is a polymer whose thermal properties are two orders of magnitude lower than those of the epoxy.

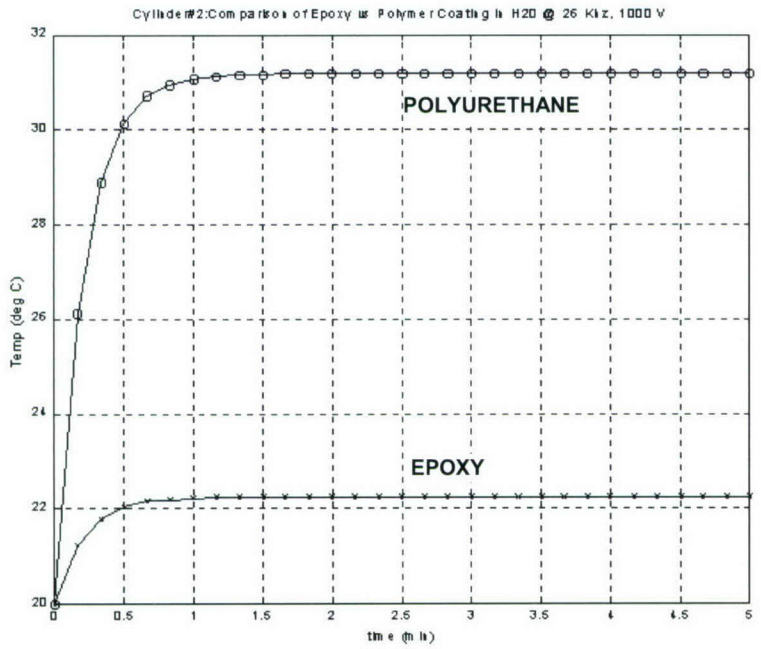

Figure 30. In-Water Model of Cylinder 2 with Epoxy Coating and Polyurethane Coating at 26 kHz (Ring Resonance) and 1000-Vrms Drive, Coating Thickness d = 0.0625 Inch (Inputs to Model: $f = 26$ kHz, $h = 1350$, $K^T = 1100$, $T_o = 20$ °C, Dissipation = 0.01, $k = 2.1$, $C_c = 420$, $\rho_c = 7600$)

Recall from equation (72) that, when h is large (as in water), the steady state is essentially determined by the thickness-to-conductivity ratio; that is,

$$T_a^{ss} - T_0 = \frac{d}{k_p} \frac{V_c Q}{A_c}. \tag{80}$$

The relative performance of the two coatings (epoxy and polyurethane) may then be expressed as the ratio of their conductivities:

$$\frac{T_P^{ss} - T_0}{T_E^{ss} - T_0} = \frac{k_E}{k_P}. \tag{81}$$

Thus, for a given thickness d, the steady-state temperatures (minus T_o) in water for two coatings of conductivity k_E and k_p are related by the ratios of their conductivities. The coating materials described in table 6 have a conductivity ratio of 5, with the steady-state values (minus T_o) in figure 30 approaching the relationship in equation (81).

8. CONCLUSIONS

The overall goal of this project is to characterize and alleviate overheating issues in the active driving piezoelectric ceramic elements and the associated passive materials used in transducer designs for high-power, compact applications. The investigation strives to identify design criteria that avoid reduced acoustic performance, reliability, and service life of a transducer caused by thermal limits. Analytical and FE models provide the means to evaluate thermal behavior during the design stage of new projector development.

The specific objective of the work reported herein was to develop analytical methods to evaluate the thermal behavior of free-flooded, 31-mode cylinder transducers. The principles developed in this report may be extended to other sonar-type transducers, such as Tonpilz and flextensional. The analytical results were confirmed by both FE methods and measurements.

The simplicity of the free-flooded, 31-mode cylinder transducer, which has both a high mechanical quality factor in air and a low quality factor in water, provided a convenient design for this investigation because it permits evaluation of the impact of material losses on heat generation both below resonance and at resonance. Through measurement and model prediction, the temperature rise in the piezoelectric material properties was dominated by the dielectric dissipation below and at resonance for the case of free-flooded, 31-mode cylinder transducers driven in water.

This report demonstrates how thermal behavior can be modeled for some simple geometries using one-dimensional, partial-differential equations. This analytical model may not apply to all cases of interest; the intent is to demonstrate the general problem and to ultimately gain a better understanding of thermal behavior.

The steady-state solution of the FE model captures the temperature profile throughout the projector at equilibrium. A steady-state solution may be used to evaluate the temperature resulting for a given duty-cycle drive by reducing dissipated power density by the percent duty cycle. For a transient solution, the thermal conduction and heat capacity of the materials must be included in an FE system of equations. The fully coupled system may then be solved for each time interval using a method of weighted residuals. The temperature rise in a transducer also causes a thermal stress, which may be taken into account using an iterative procedure, which is the subject of another investigation.

REFERENCES

1. R. Montgomery and S. C. Butler, "A Thermal Analysis of High Drive Transducer Elements," *Journal of the Acoustical Society of America*, vol. 105, no. 2, February 1999, p. 1121.

2. J. W. Waanders, "Piezoelectric Ceramic Properties and Application," Philips Components, Eindhoven, Netherlands, April 1991, p. 6.

3. S. C. Butler, "Eight Free-Flooded Ring Christmas Tree Transducer Array Acoustic Tank Measurements," NUWC-NPT Technical Memorandum 980161, Naval Undersea Warfare Center Division, Newport, RI, 8 October 1998.

4. P. J. Klippel and S. C. Butler, "Coupled Finite Element/Boundary Element Numerical Analysis of Christmas Tree Transducer Array," NUWC-NPT Technical Memorandum 990034, Naval Undersea Warfare Center Division, Newport, RI, 26 March 1998.

5. S. C. Butler and S. S. Gilardi, "Broadband High Power Expendable Sound Source Suite and Power Amplifier Design," NUWC-NPT Technical Memorandum 00-146, Naval Undersea Warfare Center Division, Newport, RI, 15 December 2000.

6. D. Berlincourt, "Piezoelectric Crystals and Ceramics," in *Ultrasonic Transducer Materials* O. E. Mattiat, ed., Plenum Press, New York, 1971, pp. 84-89.

7. "Piezoelectric Ceramics Catalog," Channel Industries Inc., Santa Barbara, CA.

8. "Piezoelectric Ceramics Catalog," EDO Corporation, Salt Lake City, UT.

9. "Guide to Modern Piezoelectric Ceramics Catalog," Morgan Matroc Inc., Bedford, OH.

10. "Piezoelectric Technology Data for Designers Catalog," Morgan Matroc Inc., Bedford, OH.

11. F. M. White, *Heat and Mass Transfer*, Addison-Wesley, Reading MA, 1988.

12. G. Arfken, *Mathematical Methods for Physicists*, Academic Press, 1985.

13. "FLUX2D Electromagnetic and Thermal Analysis 2-D Finite Element Program," Magsoft Corporation, Troy, NY.

14. G. B. Arfken, D. F. Griffing, D. C. Kelly, and J. Priest, *University Physics*, Academic Press, 1984.

15. Private Communication with Stephen E. Turner, Naval Undersea Warfare Center Division, Newport, RI.

16. J.C. Debus, "Latest Developments in ATILA Thermal Computations," *Proceedings of the 2nd Annual ATILA Workshop in U.S.*, Baltimore, MD, May 2001.

BIBLIOGRAPHY

Berlincourt, D., "Power Capacities of Piezoelectric Ceramics in Sonar-Type Acoustic Transducers," TP-221, Morgan Matroc Inc., Bedford, OH.

Berlincourt, D., "Power Limitations of Piezoelectric Ceramics in Radiating Transducers," TP-225, Morgan Matroc Inc., Bedford, OH.

Berlincourt, D., and H. Krueger, "Important Properties of Morgan Matroc Piezoelectric Ceramics," TP-226, Morgan Matroc Inc., Bedford, OH.

Boas, M. L., *Mathematical Methods in the Physical Sciences*, Second Edition, John Wiley and Sons, New York 1983.

Bronwell, A., *Advanced Mathematics in Physics and Engineering*, McGraw-Hill Book Company, New York, 1953.

Dubus, B., A. Lavie, et al., "Coupled Finite Element Boundary Element Method for the Analysis of Acoustic Scattering from Elastic Structures," *Proceedings of the 15th ASME Vibration and Noise Conference*, vol. 3 part B, 1995, pp. 25-32.

Dubus, B., and D. Boucher, "An Analytical Evaluation of the Heating of Low-Frequency Sonar Projectors," *Journal of the Acoustical Society of America*, vol. 95, no. 4, April 1994.

Dubus, B., P. Bigotte, and D. Boucher, "Thermal Limit Analysis of Low-Frequency, High-Power Sonar Projectors," *European Conference on Underwater Acoustics*, M. Weydert, ed, Elsevier Applied Science, New York, 1992, pp. 623-626.

Goodhart, C. L.,"Temperature Effects of Cement Joints in Ceramic-Stack Resonators," NOSC Technical Report 860, Naval Ocean Systems Center, San Diego, CA, June 1983.

Holland, R., "Representation of Dielectric, Elastic and Piezoelectric Losses by Complex Coefficients," *IEEE Transactions on Sonics and Ultrasonics*, vol. SU-14, no. 1, January 1967, pp. 18-20.

Lane, A. L.,"Barium Titanate Admittance-Temperature Characteristics," *Journal of the Acoustical Society of America*, vol. 25, no. 5, September 1953.

Priya, S., D. Viehland, et al., "High-Power Resonant Measurements of Piezoelectric Materials: Importance of Elastic Nonlinearities," *Journal of Applied Physics*, vol. 90, August 2001, pp. 1469-1479.

Rouquerol, E. V., "Calculation of the Heating of a Tonpilz-Type Transducer Due to the Dissipation from the Ceramic and the Geometry of the Element," ASW Laboratory, Report No. 13533, LeBrusc, France, 14 June 1965. (Translated by D. T. Porter, USL Technical Memorandum 960-32-66, U. S. Navy Underwater Sound Laboratory, New London, CT, 30 March 1966.

Shanker, N., and C. L. Hom, "An Acoustic/Thermal Model for Self-Heating in PMN Sonar Projects," *Journal of the Acoustical Society of America*, vol. 108, no. 5, November 2000.

Uchino, K., and S. Hirose, "Loss Mechanisms in Piezoelectrics: How to Measure Different Losses Separately," *IEEE Transactions on Ultrasonics, Ferroelectrics, and Frequency Control*, vol. 48, no. 1, January 2001, pp. 307-321.

Wilson, O. B., *An Introduction to the Theory and Design of Sonar Transducers*, Peninsula Publishing, Los Altos, CA, 1988.

Woollett, R. S., "Power Limitations of Sonic Transducers," *IEEE Transactions on Sonics and Ultrasonics*, vol. SU-15, no. 4, October 1968, pp. 218-229.

APPENDIX A
DECOUPLING OF THERMAL ENERGY BALANCE EQUATIONS FOR COATED CYLINDERS

The energy balances for a coated ceramic cylinder and the polymer coating are given in equations (59) and (60), respectively; they are repeated here as equations (A-1) and (A-2):

$$\rho_c C_c \frac{\partial T_a}{\partial t} V_c = Q V_c - k_p A_c \frac{T_a - T_b}{d}, \tag{A-1}$$

and

$$\frac{1}{2} V_p \rho_p C_p \frac{\partial (T_a + T_b)}{\partial t} = A_p k_p \frac{T_a - T_b}{d} - A_p h(T_b - T_\infty). \tag{A-2}$$

Equation (A-1) can be arranged as

$$\left(\frac{\partial}{\partial t} + \tau_c\right) T_a - \tau_c T_b = Q_c, \tag{A-3}$$

where

$$Q_c \equiv \frac{Q}{\rho_c C_c}, \tau_c \equiv \frac{k_p A_c}{d \rho_c C_c V_c}. \tag{A-4}$$

Similarly, rearranging equation (A-2) yields

$$\left(\frac{\partial}{\partial t} - \tau_p\right) T_a + \left(\frac{\partial}{\partial t} + \tau_p + \tau_h\right) T_b = 0, \tag{A-5}$$

where

$$\tau_p \equiv \frac{2 k_p A_p}{d \rho_p C_p V_p}, \tau_h \equiv \frac{2 h A_p}{\rho_p C_p V_p}, \tag{A-6}$$

T_∞ is assumed to approach zero, and d denotes the thickness of the coating. These constants τ_a, τ_b, τ_c, τ_h, and τ_p have units of inverse time; thus, their inverses represent a characteristic thermal relaxation time for conduction or convection. For example, $1/\tau_c$ is a measure of the relaxation time for conduction of heat from the ceramic to the coating.

For convenience, write the operators in equations (A-3) and (A-5) as a coupled system of equations:

$$D_{11}\ T_a - D_{12}\ T_b = Q_c, \tag{A-7}$$

$$D_{21}\ T_a + D_{22}\ T_b = 0, \tag{A-8}$$

where the operators are

$$D_{11} = \left(\partial/\partial t + \tau_c\right),$$

$$D_{12} = \tau_c,$$

$$D_{21} = \left(\partial/\partial t - \tau_p\right),$$

and

$$D_{22} = \left(\partial/\partial t + \tau_p + \tau_h\right).$$

Multiplying equation (A-7) by D_{22} and multiplying equation (A-8) by D_{12} and then combining the results by expressing T_b in terms of T_a yields

$$\left(D_{22}\ D_{11} + D_{12}\ D_{21}\right)T_a = D_{22}\ Q_c. \tag{A-9}$$

Carrying out the operations in this equation, using the definitions of the D's and τ's, yields

$$\left(\frac{\partial^2}{\partial t^2} + \varepsilon_1 \frac{\partial}{\partial t} + \varepsilon_2\right)T_a = \varepsilon_3 Q_c, \tag{A-10}$$

where

$$\varepsilon_1 = 2\tau_c + \tau_p + \tau_h \tag{A-11}$$

$$\varepsilon_2 = \left(\tau_p + \tau_h\right)\tau_c - \tau_c\tau_p \tag{A-12}$$

$$\varepsilon_3 = \tau_p + \tau_h. \tag{A-13}$$

Equation (A-10) is the desired energy balance equation; it is equation (61) in the body of this report.

APPENDIX B
MEASURED IN-AIR DIELECTRIC CONSTANT DISSIPATION FACTOR AND POWER

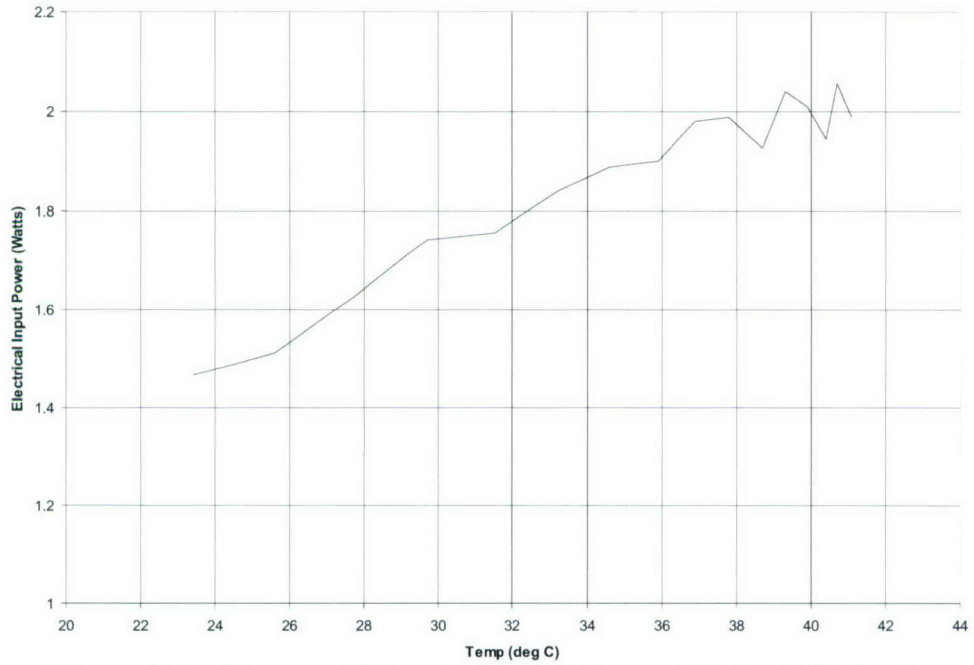

Figure B-1. Measured Electrical Input Power (W) for Cylinder 1, 750 Vrms (3.9 kV/in.) at 5 kHz in Air and No Coating

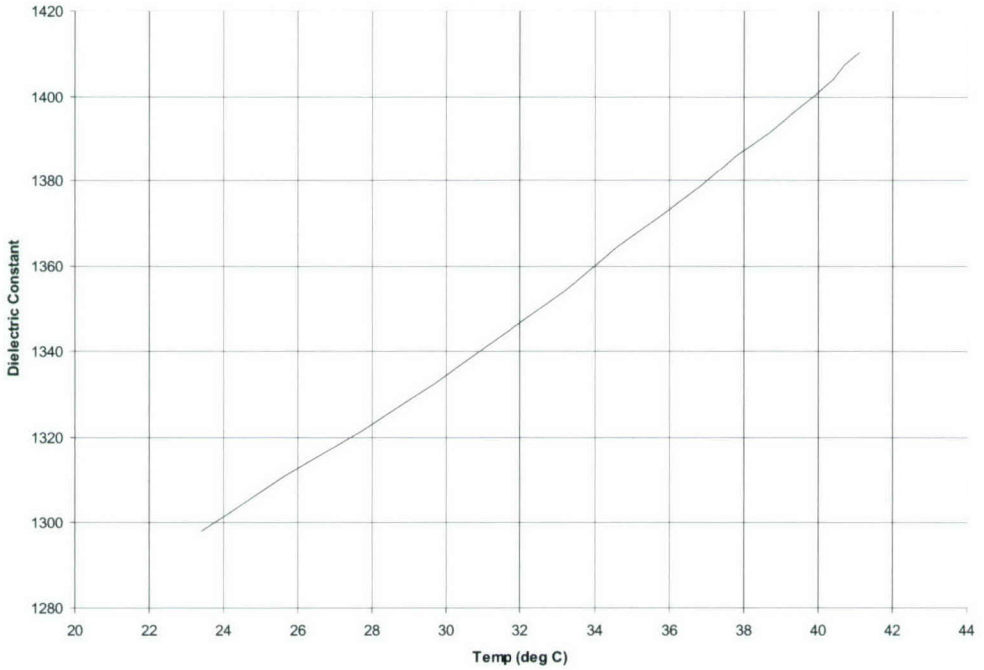

Figure B-2. Measured Dielectric Constant for Cylinder 1, 750 Vrms (3.9 kV/in.) at 5 kHz in Air and No Coating

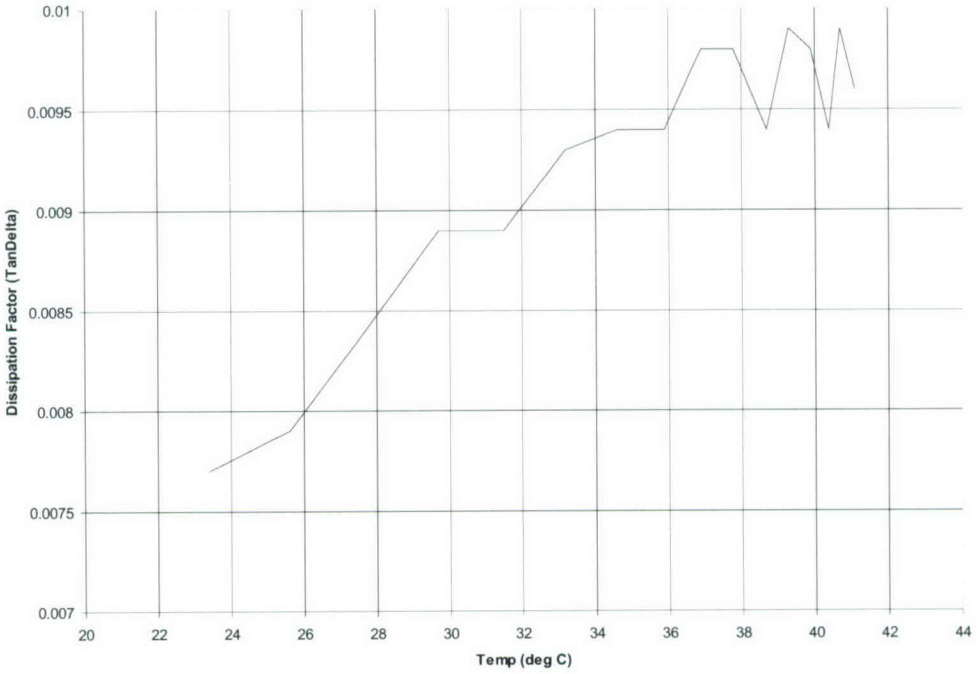

Figure B-3. Measured Electrical Dissipation Factor for Cylinder 1, 750 Vrms (3.9 kV/in.) at 5 kHz in Air and No Coating

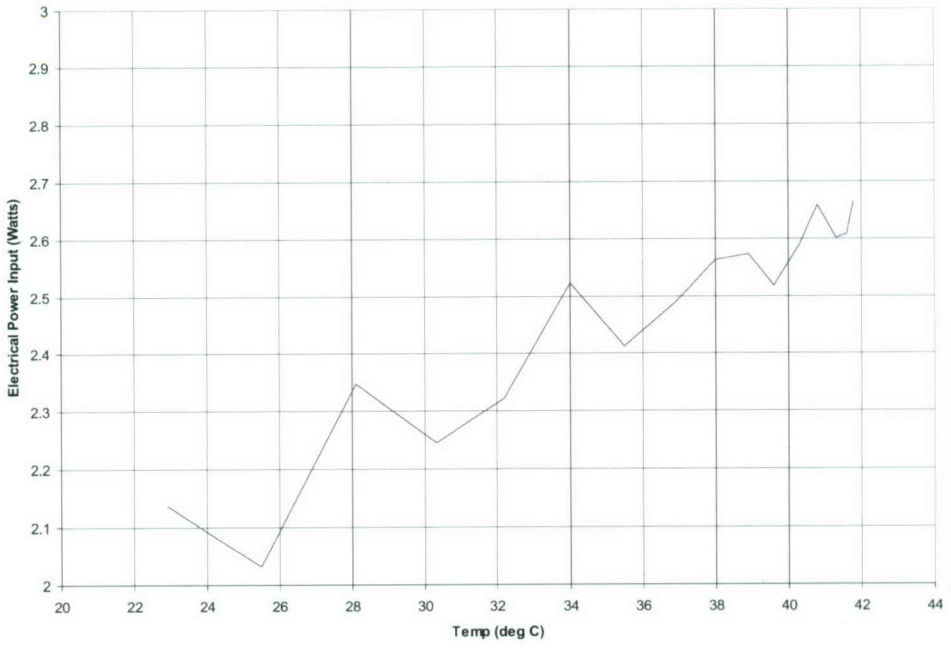

Figure B-4. Measured Electrical Input Power (W) for Cylinder 2, 1000 Vrms (5.4 kV/in.) at 10 kHz in Air and No Coating

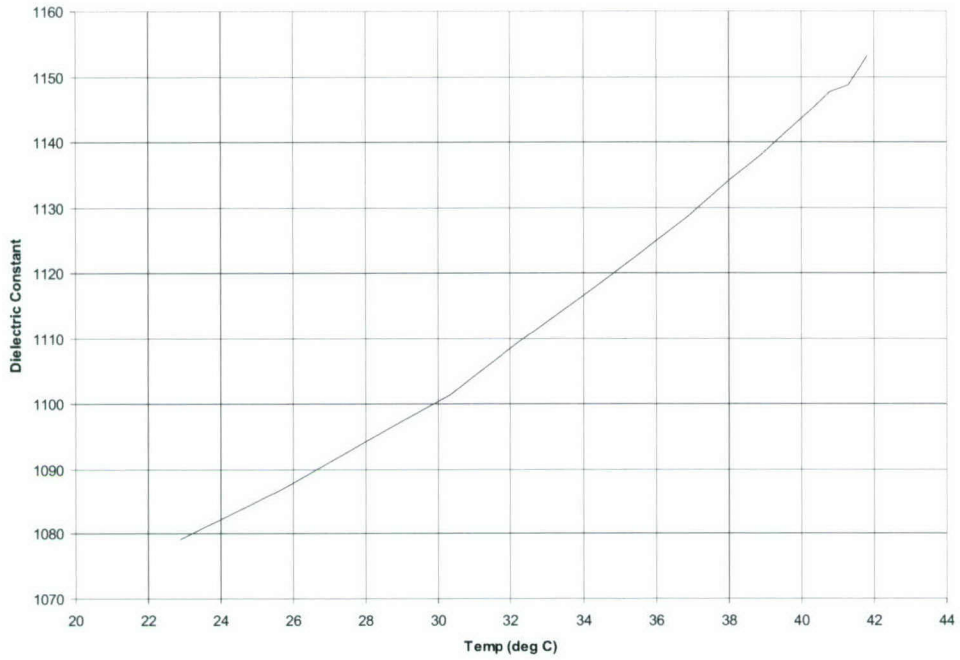

Figure B-5. Measured Dielectric Constant for Cylinder 2, 1000 Vrms (5.4 kV/in.) at 10 kHz in Air and No Coating

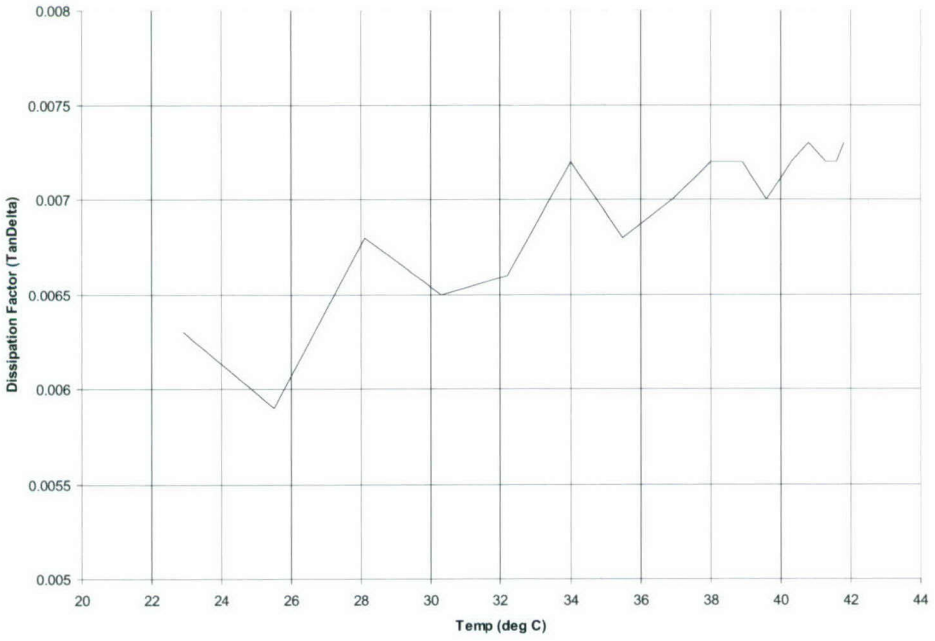

Figure B-6. Measured Electrical Dissipation Factor for Cylinder 2, 1000 Vrms (5.4 kV/in.) at 10 kHz in Air and No Coating

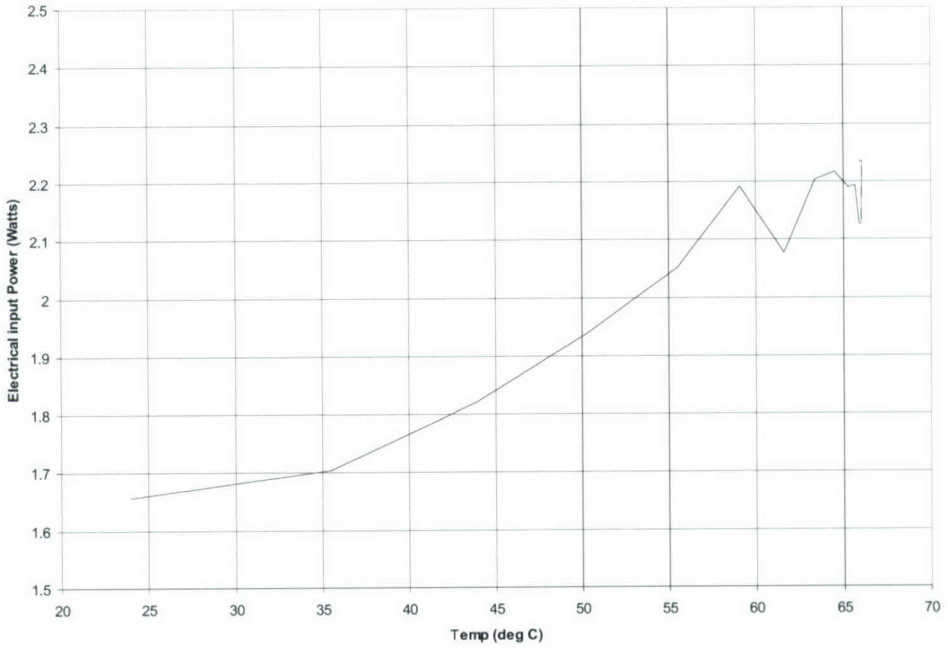

Figure B-7. Measured Electrical Input Power (W) for Cylinder 3, 1000 Vrms (7.6 kV/in.) at 10 kHz in Air and No Coating

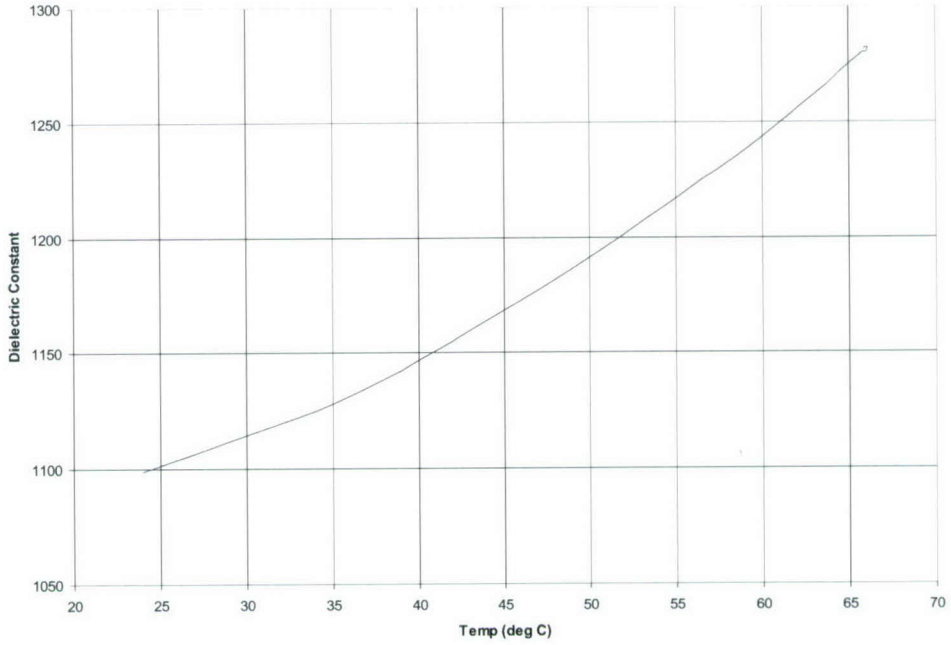

Figure B-8. Measured Dielectric Constant for Cylinder 3, 1000 Vrms (7.6 kV/in.) at 10 kHz in Air and No Coating

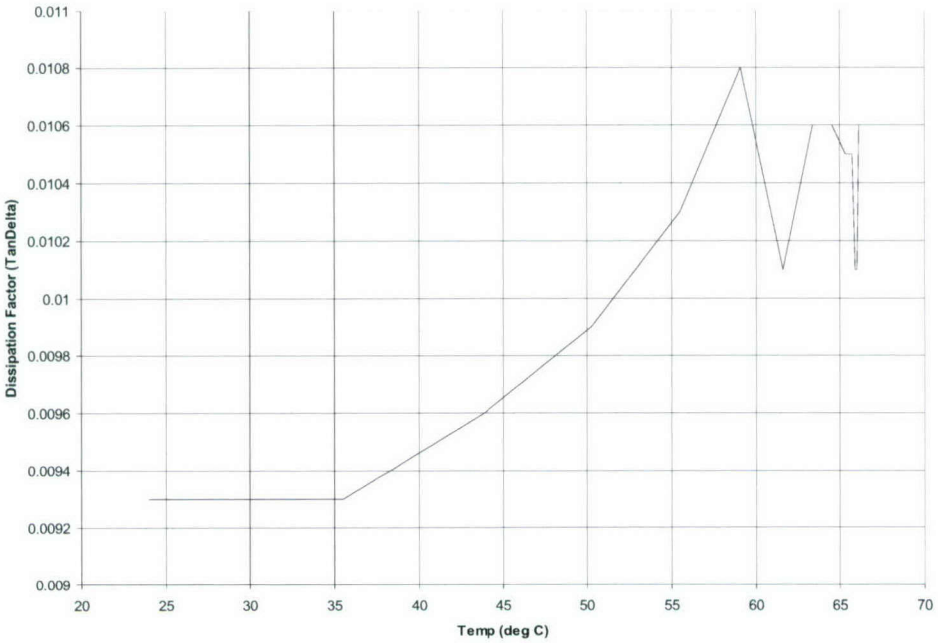

Figure B-9. Measured Electrical Dissipation Factor for Cylinder 3, 1000 Vrms (7.6 kV/in.) at 10 kHz in Air and No Coating

REPORT DOCUMENTATION PAGE

Form Approved
OMB No. 0704-0188

1. AGENCY USE ONLY *(Leave blank)*	2. REPORT DATE	3. REPORT TYPE AND DATES COVERED
	15 August 2005	

4. TITLE AND SUBTITLE

A Thermal Analysis of High-Drive Ring Transducer Elements

5. FUNDING NUMBERS

6. AUTHOR(S)

Stephen C. Butler
John B. Blottman III
Robert E. Montgomery

7. PERFORMING ORGANIZATION NAME(S) AND ADDRESS(ES)

Naval Undersea Warfare Center Division
1176 Howell Street
Newport, RI 02841-1708

8. PERFORMING ORGANIZATION REPORT NUMBER

TR 11,467

9. SPONSORING/MONITORING AGENCY NAME(S) AND ADDRESS(ES)

Office of Naval Research (ONR-333)
Ballston Centre Tower One
800 North Quincy Street
Arlington VA 22217-5660

10. SPONSORING/MONITORING AGENCY REPORT NUMBER

11. SUPPLEMENTARY NOTES

12a. DISTRIBUTION/AVAILABILITY STATEMENT

Approved for public release; distribution is unlimited.

12b. DISTRIBUTION CODE

13. ABSTRACT (Maximum 200 words)

The increasing demand for high-power, low-cost, compact transducer packages for underwater acoustic applications is leading to concerns of overheating in the active, driving piezoelectric ceramic (lead zirconate titanate) elements and the associated passive materials (epoxies and polyurethanes). Pushing a design to its thermal limits can lead to reduced acoustic performance and reliability, and the literature provides little guidance on coping with thermal issues of piezoelectric ceramics in the design phase. This report presents an analytical modeling effort that addresses the thermal issues resulting from dielectric losses for a compact, high-drive, 31-mode, free-flooded ring transducer. For this transducer, thermal issues—rather than electric field or mechanical stress—proved to be the limiting design concern. With modeling (analytical and finite element) and bench-top testing of components, however, proper materials and configuration parameters are selected and the performance goals are subsequently achieved. The approach addresses both the transient thermal response and the steady-state temperature profile that results from high-power, high-duty-cycle drive. These results may prove useful for other similar designs.

14. SUBJECT TERMS

High-Power Compact Transducers Heat Transfer Characteristics
Piezoelectric Ceramic Elements Underwater Acoustic Applications

15. NUMBER OF PAGES
62

16. PRICE CODE

17. SECURITY CLASSIFICATION OF REPORT	18. SECURITY CLASSIFICATION OF THIS PAGE	19. SECURITY CLASSIFICATION OF ABSTRACT	20. LIMITATION OF ABSTRACT
Unclassified	Unclassified	Unclassified	SAR

REPORT DOCUMENTATION PAGE

Form Approved
OMB No. 0704-0188

1. AGENCY USE ONLY *(Leave blank)*	2. REPORT DATE	3. REPORT TYPE AND DATES COVERED
	15 August 2005	

4. TITLE AND SUBTITLE

A Thermal Analysis of High-Drive Ring Transducer Elements

5. FUNDING NUMBERS

6. AUTHOR(S)

Stephen C. Butler
John B. Blottman III
Robert E. Montgomery

7. PERFORMING ORGANIZATION NAME(S) AND ADDRESS(ES)

Naval Undersea Warfare Center Division
1176 Howell Street
Newport, RI 02841-1708

8. PERFORMING ORGANIZATION REPORT NUMBER

TR 11,467

9. SPONSORING/MONITORING AGENCY NAME(S) AND ADDRESS(ES)

Office of Naval Research (ONR-333)
Ballston Centre Tower One
800 North Quincy Street
Arlington VA 22217-5660

10. SPONSORING/MONITORING AGENCY REPORT NUMBER

11. SUPPLEMENTARY NOTES

12a. DISTRIBUTION/AVAILABILITY STATEMENT

Approved for public release; distribution is unlimited.

12b. DISTRIBUTION CODE

13. ABSTRACT (Maximum 200 words)

The increasing demand for high-power, low-cost, compact transducer packages for underwater acoustic applications is leading to concerns of overheating in the active, driving piezoelectric ceramic (lead zirconate titanate) elements and the associated passive materials (epoxies and polyurethanes). Pushing a design to its thermal limits can lead to reduced acoustic performance and reliability, and the literature provides little guidance on coping with thermal issues of piezoelectric ceramics in the design phase. This report presents an analytical modeling effort that addresses the thermal issues resulting from dielectric losses for a compact, high-drive, 31-mode, free-flooded ring transducer. For this transducer, thermal issues—rather than electric field or mechanical stress—proved to be the limiting design concern. With modeling (analytical and finite element) and bench-top testing of components, however, proper materials and configuration parameters are selected and the performance goals are subsequently achieved. The approach addresses both the transient thermal response and the steady-state temperature profile that results from high-power, high-duty-cycle drive. These results may prove useful for other similar designs.

14. SUBJECT TERMS

High-Power Compact Transducers Heat Transfer Characteristics
Piezoelectric Ceramic Elements Underwater Acoustic Applications

15. NUMBER OF PAGES

62

16. PRICE CODE

17. SECURITY CLASSIFICATION OF REPORT	18. SECURITY CLASSIFICATION OF THIS PAGE	19. SECURITY CLASSIFICATION OF ABSTRACT	20. LIMITATION OF ABSTRACT
Unclassified	Unclassified	Unclassified	SAR

INITIAL DISTRIBUTION LIST

Addressee	No. of Copies
Office of Naval Research (ONR-321 (M. Vacarro, J, Lindberg, T. McMullen), ONR-33 (R. Pohanka), ONR-332 (W. Smith), ONR-333 A. Nucci)	6
SPAWAR Systems Center (D. Gillette, W. Rask, J. DeJaco)	3
Pennsylvania State University/Applied Research Laboratory (J. Hughs, C. Allen, T. Gabrielson, R. Meyers, T. Montgomery)	5
L3 Communications Inc. (S. Hudson)	1
ITC Corporation (E. Knutsal, W. Bunker)	2
Image Acoustics Inc. (J. Butler, A. Butler)	2
Massa Products Corporation (D. Massa, G. Cavanaugh, R. Hennebury)	3
Raytheon Company (D. Roberti, W. Marshall, P. Brogan)	3
Ultra Electronics, Ocean Systems Inc. (R. Laron, J. Bidorini, E. Guida)	3
BAE Systems, Sanders (J. Osborn, M. Deangelis)	2
Northrop Grumman Corporation (L. Rowe, F. Geil)	2
Harris Acoustic Products Corporation (W. Pozzo, T. Baldasarre)	2
EDO Corporation	1
Material Systems Inc. (L. Bowen, B. Doust)	2
Lockheed Martin Corporation (R. Porzio, D. Erickson)	2
Progeny Systems Inc. (J. Powers, D. Baird)	2
Defense Technical Information Center	2
Center for Naval Analyses	1